Fast Contingency Analysis and Control for Overload Mitigation in Integrated High Voltage AC and Multi-Terminal HVDC Grids

Kai Strunz, Samuel Schilling, Maren Kuschke, and Anna Czerwinska

***Abstract*—The increasing integration of renewable energy sources calls for an extension of transmission capacity for transporting power towards load centers. Given the involved distances, the integration of high voltage DC connections into AC transmission grids becomes a reality. The interest in such AC-DC transmission grids has been further driven by the potential of multi-terminal HVDC grids interfaced via voltage sourced converters. Their capability of power flow control can contribute to overload mitigation, especially also in case of contingencies. In security analysis of AC grids, the application of linear sensitivity methods for very fast analysis of various contingencies has become established. In this article such contingency analysis is developed for integrated AC-DC transmission grids. Power transfer distribution and line outage distribution factors are reformulated to yield the novel AC-DC power transfer compensation and line outage compensation factors. Those account for the fact that voltage sourced converters allow for controlling power flows. A further innovation is the optimization for the fast identification of AC-DC voltage sourced converter operating point adjustments to mitigate system-wide overloads. Accuracy, principal functionality, robustness, and computational efficiency of the proposed methodology are demonstrated. Scenarios were studied on a modified IEEE 39-bus system and a hypothetical future German power grid.**

***Index Terms*—Congestion management, contingency analysis, HVDC control, HVDC transmission, integrated AC-DC power system, interior-point method, linear power flow calculation, linear sensitivity method, multi-terminal HVDC system, power system security, voltage sourced converter.**

NOMENCLATURE

Selected abbreviations

HVDC	High voltage direct current.
LOCF	Line outage compensation factor.
LODF	Line outage distribution factor.
PTCF	Power transfer compensation factor.
PTDF	Power transfer distribution factor.
p.u.	Per unit.
RMS	Root-mean-square.
VSC	Voltage sourced converter.

Sets

$\mathscr{B}$	Buses to which outaged generators, loads, or VSCs are connected.
$\mathscr{L}$	Outaged lines.

Subscripts, superscripts, and stacked identifiers

AC	Referring to AC grid.
ctl	Quantity modified by control.
DC	Referring to DC grid.
lim	Limit of quantity.
0	Initial quantity.
$\sim$	Quantity modified by outage.

Selected mathematical symbols

$\boldsymbol{B}$	Susceptance matrix.
c_{ik}	Coupling term of bus i and VSC k.
$\boldsymbol{CCM}$	Congestion compensation matrix.
$\boldsymbol{G}$	Conductance matrix.
$\boldsymbol{I}_{n_{\text{conv}}}$	Identity matrix of dimension $n_{\text{conv}} \times n_{\text{conv}}$.
$LOCF_{lmk}$	Sensitivity of power flow change on line l to change of injection by VSC k during outage of line m.
$LODF_{lm}$	Sensitivity of power flow change on line l to outage of line m.
n_{b}	Number of buses.
n_{conv}	Number of VSCs.
n_{l}	Number of lines.
$P_{\text{ACDC},k}$	Real power injection from AC to DC grid part through VSC k.
$P_{\text{DCAC},k}$	Real power injection from DC to AC grid part through VSC k.
P_i^{gen}	Real power of generator at bus i.
P_i^{inj}	Net real power injection into bus i.
P_i^{load}	Real power of load at bus i.
P_l	Real power flow over line l.
$P_{\text{loss},k}$	Conversion power losses of VSC k.
$PTCF_{lk}$	Sensitivity of power flow change on line l to change of power injection by VSC k.
$PTDF_{lsr}$	Sensitivity of power flow change on line l to shift of injection from bus s to bus r.
$\boldsymbol{R}$, R_{ij}	Resistance matrix, resistance matrix element.
r_{ij}	Line resistance between buses i and j.
V_i	Voltage at bus i.
v_i	Difference between voltage at bus i and voltage at reference bus.
$\boldsymbol{X}$, X_{ij}	Reactance matrix, reactance matrix element.
x_{ij}	Line reactance between buses i and j.
θ_i	Voltage phase angle at bus i.
$\boldsymbol{\sigma}_{1\times n_{\text{conv}}}^{\top}$	Vector of ones of dimension $1 \times n_{\text{conv}}$.
$\boldsymbol{0}_{n_{\text{conv}}}$	Zero matrix of dimension $n_{\text{conv}} \times n_{\text{conv}}$.
$\boldsymbol{0}_{1\times n_{\text{conv}}}$	Zero matrix of dimension $1 \times n_{\text{conv}}$.
$\Delta\xi$	Change of quantity ξ.

Manuscript received xxxx xx, 2023. This work was supported by the German Federal Ministry for Economic Affairs and Energy (BMWi) within the project OVANET2.0 (no. 0350037A).

M. Kuschke, A. Czerwinska, and K. Strunz are with the Technische Universität Berlin, Berlin 10587, Germany (e-mail: kai.strunz@tu-berlin.de), S. Schilling is with 50Hertz Transmission GmbH

I. INTRODUCTION

BY 2021, the global wind power capacity has increased to 837 GW, whereas 93 GW were installed in 2021 alone [1]. As wind farms are typically located where wind power potential is significant, grid extension is among the solutions considered to bridge the distance to the load centers. To achieve higher public acceptance for grid extension, the usage of underground power cables is given serious consideration in a number of countries, as for example in Germany. Here, power transmission by high voltage DC (HVDC) underground cable is seen as a promising option as no reactive power compensation is

needed [2], [3]. The interest in HVDC power transmission has been stimulated further by the capabilities of multi-terminal DC structures based on the voltage sourced converter (VSC) [4]–[9]. The integration of VSC-based DC structures enables the grid operator to modify the power flow [10]–[12].

Yet, the operation of an integrated AC-DC grid also brings new challenges. A key challenge is the system-wide security analysis. To address this point, inspiration can be taken from the security analysis of existing AC power systems. According to [13], the issue of power system security covers the following three major functions: system monitoring, contingency analysis, and security-constrained optimal power flow. System monitoring provides the system operator with online information on the current state of the power grid [14], [15]. Security-constrained optimal power flow calculation determines redispatch measures to counteract critical grid conditions [16]–[19]. Contingency analysis is aimed at the quick evaluation of a large number of scenarios in order to identify potentially critical outages. As explained in [13] and [20], linear power flow calculation is considered as an appropriate basis for contingency analysis of AC transmission grids when the main focus is on approximate but very fast algorithms.

With the increasing interest in integrated AC and multi-terminal DC transmission grids, the according extension of linear power flow algorithms has attracted attention [21]. Linear power flow analysis lends itself to the formulation of linear sensitivity methods, which facilitate computationally efficient contingency analysis. In [12], sensitivity factors are based on the first-order Taylor series approximation, yet the power flow calculation itself remains iterative. A linear and non-iterative application of sensitivity factors for contingency analysis was demonstrated in [22].

In this work, linear sensitivity methods are found to be useful in the analysis of contingencies, too. But beyond a contingency analysis that considers settings of controllers to be constant as for example in [22], the proposed methodology also includes a contingency control technique. The latter is capable of adjusting control settings of integrated AC-DC power systems with the aim to mitigate contingencies. The focus here is on the setting of VSC controls, as those are accessible by Transmission System Operators. To this effect, there are three complementary contributions. First, novel power transfer compensation and line outage compensation factors for integrated AC and multi-terminal DC transmission grids are developed. Those factors define the sensitivity of the line power flow to a controlled change of power injection by an AC-DC converter in the wake of a contingency. Second, a control strategy of the AC-DC converters with the objective to mitigate a detected contingency-triggered overload is formulated as an optimization problem, and the solution process is shown. Third, the performance of the contingency analysis and control is thoroughly evaluated in terms of accuracy and robustness, and the computational efficiency is verified.

The remainder of this paper is structured as follows. The linear calculation of power flows in an AC-DC grid is considered in Section II. In Section III, the linear sensitivity factors for AC-DC grids considering the opportunity of controlling VSC operating points are developed. In Section IV, the optimization problem to mitigate the detected overload is formulated, based on the previously defined sensitivity factors. The accuracy, functionality, and robustness of the proposed method are evaluated in Section V. In Section VI, the computational efficiency when applied to a realistic large-scale power system is confirmed by a case study of a hypothetical future German AC-DC power grid. In Section VII, conclusions are drawn.

II. Preparation

In what follows, relevant background information is given. The linear calculation of the power flows of AC and DC grids is revisited in Section II-A. In Section II-B, the linear power flow equations are formulated for integrated AC-DC transmission grids, which will later form a basis for the proposed contingency analysis. Without loss of generality, with the exception of the voltage angles, the following quantities are expressed in the per unit (p.u.) system.

A. Linear Power Flow Calculation of Independent AC and DC Transmission Grids in Normal Operation

As described for example in [13], linear power flow calculation achieves a level of accuracy that makes it practical for contingency analysis for a wide range of operating conditions in electric power transmission systems. For this purpose, power flow equations of an AC grid are linearized by assuming small differences of bus voltage phase angles, neglecting the resistances and shunt capacitances of transmission lines, and setting all voltage magnitudes to 1 p.u.. The power equality constraints for each bus i under these assumptions are

$$P_{\mathrm{AC},i}^{\mathrm{inj}} = P_{\mathrm{AC},i}^{\mathrm{gen}} - P_{\mathrm{AC},i}^{\mathrm{load}} \tag{1}$$

$$P_{\mathrm{AC},i}^{\mathrm{inj}} = \sum_{j=1}^{n_{\mathrm{b,AC}}} \frac{\theta_{\mathrm{AC},i} - \theta_{\mathrm{AC},j}}{x_{\mathrm{AC},ij}} \tag{2}$$

where $P_{\mathrm{AC},i}^{\mathrm{inj}}$ is the net real power injection into bus i determined by the difference of real generator power $P_{\mathrm{AC},i}^{\mathrm{gen}}$ and real load power $P_{\mathrm{AC},i}^{\mathrm{load}}$; $x_{\mathrm{AC},ij}$ is the reactance of the transmission line between AC buses i and j; $\theta_{\mathrm{AC},i}$ and $\theta_{\mathrm{AC},j}$ are the voltage phase angles at buses i and j.

In a DC grid with $n_{\mathrm{b,DC}}$ buses, the power equality constraints for each bus i are given by

$$P_{\mathrm{DC},i}^{\mathrm{inj}} = P_{\mathrm{DC},i}^{\mathrm{gen}} - P_{\mathrm{DC},i}^{\mathrm{load}} \tag{3}$$

$$P_{\mathrm{DC},i}^{\mathrm{inj}} = V_{\mathrm{DC},i} \sum_{j=1}^{n_{\mathrm{b,DC}}} \frac{V_{\mathrm{DC},i} - V_{\mathrm{DC},j}}{r_{\mathrm{DC},ij}} \tag{4}$$

where $P_{\mathrm{DC},i}^{\mathrm{inj}}$ is the net real power injection into bus i determined by the difference of real generator power $P_{\mathrm{DC},i}^{\mathrm{gen}}$ and real load power $P_{\mathrm{DC},i}^{\mathrm{load}}$; $r_{\mathrm{DC},ij}$ is the resistance of the transmission line between DC buses i and j; $V_{\mathrm{DC},i}$ and $V_{\mathrm{DC},j}$ are the voltages at buses i and j.

Equation (4) may be linearized by assuming $V_{\mathrm{DC},i}(V_{\mathrm{DC},i} - V_{\mathrm{DC},j}) \approx V_{\mathrm{DC},i} - V_{\mathrm{DC},j}$ [21], [23], [24]. This leads to

$$P_{\mathrm{DC},i}^{\mathrm{inj}} = \sum_{j=1}^{n_{\mathrm{b,DC}}} \frac{v_{\mathrm{DC},i} - v_{\mathrm{DC},j}}{r_{\mathrm{DC},ij}} \tag{5}$$

where $v_{\mathrm{DC},i}$ and $v_{\mathrm{DC},j}$ are the voltage differences between the bus voltages $V_{\mathrm{DC},i}$ and $V_{\mathrm{DC},j}$ and the voltage $V_{\mathrm{DC,ref}}$ at the DC reference bus, respectively.

Defining one reference bus each for the AC and DC grids, respectively, the power equality constraints of (2) and (5) are rewritten in matrix form

$$\boldsymbol{P}_{\mathrm{AC}}^{\mathrm{inj}} = \boldsymbol{B}_{\mathrm{AC}}\boldsymbol{\theta}_{\mathrm{AC}} \tag{6a}$$

$$\boldsymbol{P}_{\mathrm{DC}}^{\mathrm{inj}} = \boldsymbol{G}_{\mathrm{DC}}\boldsymbol{v}_{\mathrm{DC}} \tag{6b}$$

where $\boldsymbol{P}_{\text{AC}}^{\text{inj}}$ is the vector of the power injections into all AC buses except for the AC reference bus; $\boldsymbol{\theta}_{\text{AC}}$ is the vector of voltage angles at all AC buses except for the AC reference bus; $\boldsymbol{P}_{\text{DC}}^{\text{inj}}$ is the vector of the power injections into all DC buses except for the DC reference bus; entries of $\boldsymbol{v}_{\text{DC}}$ are the deviations of the bus voltages from the voltage at the DC reference bus; $\boldsymbol{B}_{\text{AC}}$ and $\boldsymbol{G}_{\text{DC}}$ are composed of the following elements:

$$B_{\text{AC},ik} = \begin{cases} \sum_{\substack{j=1 \\ j\neq i}}^{n_{\text{b,AC}}} \frac{1}{x_{\text{AC},ij}}, & \text{if} \quad k = i \\ -\frac{1}{x_{\text{AC},ik}}, & \text{if} \quad k \neq i \end{cases} \tag{7a}$$

$$G_{\text{DC},ik} = \begin{cases} \sum_{\substack{j=1 \\ j\neq i}}^{n_{\text{b,DC}}} \frac{1}{r_{\text{DC},ij}}, & \text{if} \quad k = i \\ -\frac{1}{r_{\text{DC},ik}}, & \text{if} \quad k \neq i. \end{cases} \tag{7b}$$

After building preliminary matrices according to (7a) and (7b) for all $i, k \in \{1, ..., n_{\text{b,AC}}\}$ or $i, k \in \{1, ..., n_{\text{b,DC}}\}$, the rows and columns corresponding to AC and DC reference buses are removed to obtain $\boldsymbol{B}_{\text{AC}}$ and $\boldsymbol{G}_{\text{DC}}$. This step is necessary to obtain matrices that are invertible.

The voltage at the DC reference bus is set to 1 p.u., whereas the voltage angle at the AC reference bus is set to $0°$. For all other buses, the voltage angles at AC buses and the voltages at DC buses are then analytically expressed by

$$\boldsymbol{\theta}_{\text{AC}} = \boldsymbol{X}_{\text{AC}} \boldsymbol{P}_{\text{AC}}^{\text{inj}} \tag{8a}$$

$$\boldsymbol{v}_{\text{DC}} = \boldsymbol{R}_{\text{DC}} \boldsymbol{P}_{\text{DC}}^{\text{inj}} \tag{8b}$$

where $\boldsymbol{X}_{\text{AC}}$ and $\boldsymbol{R}_{\text{DC}}$ are composed of elements $X_{\text{AC},ik}$ and $R_{\text{DC},ik}$, and constitute inverses of $\boldsymbol{B}_{\text{AC}}$ and $\boldsymbol{G}_{\text{DC}}$, respectively. After solving (8a) and (8b), the power flows in p.u. over line l connecting buses i and j are obtained by

$$P_{\text{AC},l} = \frac{\theta_{\text{AC},i} - \theta_{\text{AC},j}}{x_{\text{AC},ij}} \tag{9a}$$

$$P_{\text{DC},l} = \frac{v_{\text{DC},i} - v_{\text{DC},j}}{r_{\text{DC},ij}}. \tag{9b}$$

By definition, $P_{\text{AC},l}$ and $P_{\text{DC},l}$ are positive if power flows from bus i to bus j.

B. Linear Power Flow Calculation of Integrated AC-DC Transmission Grids in Normal Operation

For the analysis of AC-DC grids, the initially independent power flow calculations for AC and DC grids are integrated by considering power exchanges through AC-DC converters. Thus, power injections of AC-DC converters are added to the bus power injections given in (1) and (3):

$$P_{\text{AC},i}^{\text{inj}} = P_{\text{AC},i}^{\text{gen}} - P_{\text{AC},i}^{\text{load}} + c_{\text{AC},ik} P_{\text{DCAC},k} \tag{10a}$$

$$P_{\text{DC},i}^{\text{inj}} = P_{\text{DC},i}^{\text{gen}} - P_{\text{DC},i}^{\text{load}} + c_{\text{DC},ik} P_{\text{ACDC},k} \tag{10b}$$

where i denotes an arbitrary AC bus or an arbitrary DC bus; $P_{\text{DCAC},k}$ is the power injection into the AC grid part through converter k; $P_{\text{ACDC},k}$ is the power injection into the DC grid part through converter k; the coupling term $c_{\text{AC},ik}$, or respectively $c_{\text{DC},ik}$, is 1 if converter k is connected to bus i, and it is 0 otherwise.

To emphasize that the operating points of converters k can be adjusted according to specified objectives or requirements of the grid operator, the following definition is introduced:

$$P_{\text{DCAC},k} = P_{\text{DCAC},k}^{0} + \Delta P_{\text{DCAC},k} \tag{11a}$$

$$P_{\text{ACDC},k} = P_{\text{ACDC},k}^{0} + \Delta P_{\text{ACDC},k} \tag{11b}$$

where $P_{\text{DCAC},k}^{0}$ and $P_{\text{ACDC},k}^{0}$ are initial power injections into the AC grid part and the DC grid part, respectively; $\Delta P_{\text{DCAC},k}$ and $\Delta P_{\text{ACDC},k}$ are changes of the power injections into the AC grid part and into the DC grid part, respectively.

Further, the following power equality constraints apply:

$$P_{\text{DCAC},k}^{0} + P_{\text{ACDC},k}^{0} + P_{\text{loss},k}^{0} = 0 \tag{12}$$

$$\Delta P_{\text{DCAC},k} + \Delta P_{\text{ACDC},k} + \Delta P_{\text{loss},k} = 0 \tag{13}$$

where $P_{\text{loss},k}^{0}$ denotes the power conversion losses of converter k at initial operating point; $\Delta P_{\text{loss},k}$ gives the changes of power conversion loss when adapting the converter operating point. Given that in this work the focus is on contingency analysis based on the linear power flow formulation, losses of power conversion are discarded.

Without loss of generality, it is assumed that power balance in the AC grid part is guaranteed by an AC reference bus, whereas an arbitrary AC-DC converter k ensures power balance in the DC grid part. Thus, in an AC-DC grid with n_{conv} converters, the initial power injection of converter k into the DC grid part is given by the power equality constraint:

$$P_{\text{ACDC},k}^{0} = -\sum_{i=1}^{n_{\text{b,DC}}} (P_{\text{DC},i}^{\text{gen}} - P_{\text{DC},i}^{\text{load}}) - \sum_{\substack{j=1 \\ j\neq k}}^{n_{\text{conv}}} P_{\text{ACDC},j}^{0}. \tag{14}$$

When adapting the AC-DC converter operating points, the changes of power injections are related as follows, since the losses are neglected:

$$\sum_{k=1}^{n_{\text{conv}}} \Delta P_{\text{ACDC},k} = 0. \tag{15}$$

For the integrated AC-DC grid, the power flows over an AC or DC line l are determined by inserting (10a) or (10b) into (8a) or (8b), and then using the obtained angles or voltages in (9a) or (9b), respectively.

III. Linear Sensitivity Factors for Outages and Overload Mitigation

Outages of generators, loads, and lines are examples for contingencies that affect the power flow. The challenge of evaluating a high number of potential outages is central to contingency analysis. The application of linear sensitivity factors for overload detection in AC transmission grids was shown to be suitable in this context [13], [25], [26]. Therefore, linear sensitivity factors lay the foundation for the methodology. As such, an essential preparatory stage of the contingency analysis is the calculation of sensitivity factors that measure the impact of changes of nodal power injections and of line outages. Those two sensitivity factors are formulated in Section III-A for AC and DC grids, respectively.

All underlying mathematical models are expressed through algebraic equations, and therefore differential equations are not involved. Following a contingency, it is assumed that transient stability is given [27], [28] so that a new steady state is reached following the outage. As long as this new steady state does not show overloads, the original power flow settings for the AC-DC converters can be maintained. If those original settings entail an overload following the outage and if a modification of the settings allows for mitigating the overload, then those settings are to be modified. Consequently, an interaction between AC and DC grid parts is observed as a result of the contingency. In order to describe the sensitivity of power flows thanks to AC-DC converter control during an outage, the so-called compensation factors are developed in Section III-B.

A. Linear Sensitivity Factors for Outages

In what follows, the detection of contingency-triggered overloads is described. At first, outages of generators and loads are considered, and sensitivity factors for overload detection are addressed. In addition, the formulations involve the detection of overloads as a consequence to outages of AC-DC converters. Secondly, line outages and the associated sensitivity factors measuring the changes of flows are considered.

1) Power Transfer Distribution Factor: In case of outages of generators or loads, power injections need to be shifted to ensure power balance in the grid. Power injections may be shifted to another bus or are distributed. Due to the shifting, the changed power flows may cause line overloads. The power transfer distribution factor (PTDF) measures the change of the flow on a line to a shift of power injection:

$$PTDF_{lsr} = \left.\frac{\Delta P_l}{\Delta P_{sr}^{\text{inj}}}\right|_{s\in\mathscr{B}} \tag{16}$$

where $\Delta P_{sr}^{\text{inj}}$ is the shift of power injection from a sending bus s to a receiving bus r; ΔP_l is the change of the power flow over line l connecting bus i and bus j; $\mathscr{B}$ is the set of buses to one of which the malfunctioning generator, load, or AC-DC converter were connected initially. By definition, $\Delta P_{sr}^{\text{inj}}$ is negative if the net real power injection into bus s is decreased, while the injection into bus r is increased; ΔP_l is positive if the power flow from bus i to bus j increases due to the shift of power injection.

If no receiving bus is specified, then the latter becomes the reference bus by definition. As such, (16) is rewritten as:

$$PTDF_{ls} = \left.\frac{\Delta P_l}{\Delta P_{s}^{\text{inj}}}\right|_{s\in\mathscr{B}} \tag{17}$$

According to [13], the $PTDF_{sl}$ for AC grids is calculated by

$$PTDF_{\text{AC},ls}=\frac{1}{x_{\text{AC},ij}}(X_{\text{AC},is}-X_{\text{AC},js}). \tag{18}$$

Analogously, it follows for DC grids according to Appendix A:

$$PTDF_{\text{DC},ls}=\frac{1}{r_{\text{DC},ij}}(R_{\text{DC},is}-R_{\text{DC},js}). \tag{19}$$

If specific receiving buses as in (16) are given, then (18) and (19) are complemented by $PTDF_{\text{AC},lr}$ and $PTDF_{\text{DC},lr}$ as follows:

$$PTDF_{\text{AC},lsr} = PTDF_{\text{AC},ls} - PTDF_{\text{AC},lr} \tag{20}$$

$$PTDF_{\text{DC},lsr} = PTDF_{\text{DC},ls} - PTDF_{\text{DC},lr} \tag{21}$$

with:

$$PTDF_{\text{AC},lr}=\frac{1}{x_{\text{AC},ij}}(X_{\text{AC},ir}-X_{\text{AC},jr}) \tag{22}$$

$$PTDF_{\text{DC},lr}=\frac{1}{r_{\text{DC},ij}}(R_{\text{DC},ir}-R_{\text{DC},jr}). \tag{23}$$

If the power injection is from bus s to the reference bus, the altered power flows over an AC line l or a DC line l at initial converter operating points are specified by

$$\widetilde{P}_{\text{AC},l}\big|_{s\in\mathscr{B}_{\text{AC}}} = P_{\text{AC},l}^0 + PTDF_{\text{AC},ls}\Delta P_{\text{AC},s}^{\text{inj}} \tag{24a}$$

$$\widetilde{P}_{\text{DC},l}\big|_{s\in\mathscr{B}_{\text{DC}}} = P_{\text{DC},l}^0 + PTDF_{\text{DC},ls}\Delta P_{\text{DC},s}^{\text{inj}} \tag{24b}$$

where $P_{\text{AC},l}^0$ and $P_{\text{DC},l}^0$ are the initial flows over the line l on the AC or DC sides; $\Delta P_{\text{AC},s}^{\text{inj}}$ and $\Delta P_{\text{DC},s}^{\text{inj}}$ are the shifts of power injections in the AC and DC grid parts.

Apart from considering the impact of changes of power injections due to outages of generators or loads, the PTDFs for AC and DC grids may also be applied for overload detection due to converter outages in an AC-DC grid. The outage of an AC-DC converter is modeled as simultaneous shifts of power injections in the AC and DC grid parts considering the power equality constraints of (12) and (13). Given the outage of a converter k, the shifts of power injections from the AC grid part to the DC grid part and vice versa are specified by $\Delta P_{\text{ACDC},k} = -P_{\text{ACDC},k}^0$ and $\Delta P_{\text{DCAC},k} = -P_{\text{DCAC},k}^0$, respectively. Taking into account the power equality constraint of (15), power balance in the AC and DC grid parts is ensured by adapting the operating point of at least one other converter. Without loss of generality, it is assumed here that the malfunctioning converter k is connected to bus s. The changes of power injections at bus s are then given by

$$\Delta P_{\text{AC},s}^{\text{inj}} = -c_{\text{AC},sk}P_{\text{DCAC},k}^0 \tag{25a}$$

$$\Delta P_{\text{DC},s}^{\text{inj}} = -c_{\text{DC},sk}P_{\text{ACDC},k}^0 \tag{25b}$$

where $c_{\text{AC},sk}$ and $c_{\text{DC},sk}$ are coupling terms introduced in (10a) and (10b). Inserting the above changes of power injections into (24a) and (24b), the altered power flows over an AC line l or a DC line l are obtained.

2) Line Outage Distribution Factor: Apart from shifts of power injection, overloads may also be triggered through line outages. As described in [13], the line outage distribution factor (LODF) measures the change of power flow:

$$LODF_{lm} = \left.\frac{\Delta P_l}{P_m^0}\right|_{m\in\mathscr{L}} \tag{26}$$

where P_m^0 is the prefault power flow over line m; $\mathscr{L}$ is the set of outaged lines; ΔP_l again is the change of flow over line l. The calculations of the LODF for AC and of the reformulated LODF for DC grids are detailed in Appendix B.

Given the outage of a line m in the AC part or the DC part of the AC-DC grid, the altered power flow over line l at initial converter operating points is specified by

$$\widetilde{P}_{\text{AC},l}\big|_{m\in\mathscr{L}_{\text{AC}}} = P_{\text{AC},l}^0 + LODF_{\text{AC},lm}P_{\text{AC},m}^0 \tag{27a}$$

$$\widetilde{P}_{\text{DC},l}\big|_{m\in\mathscr{L}_{\text{DC}}} = P_{\text{DC},l}^0 + LODF_{\text{DC},lm}P_{\text{DC},m}^0 \tag{27b}$$

where $P_{\text{AC},m}^0$ and $P_{\text{DC},m}^0$ are the prefault power flows over the line m in the AC or DC grid parts; $LODF_{\text{AC},lm}$ and $LODF_{\text{DC},lm}$ are the LODFs for the AC and DC grid parts.

Equations (24a) and (27a) are applied to calculate the modified power flow over an AC line in case of a generator, line, or converter outage in the AC part of the grid. On the other hand, equations (24b) and (27b) are applied to calculate the modified power flow over a DC line in case of a generator, line, or converter outage in the DC part of the grid. Under the assumption that the converter operating points are fixed, an outage in the AC grid part will have no influence on the DC grid part and vice versa. Such a reciprocal impact is observed if the converter operating points are variable.

B. Linear Sensitivity Factors for Overload Mitigation

While the application of the PTDF and the LODF is just for the overload detection, the concept of linear sensitivity factors is here further developed to consider overload mitigation in AC-DC grids. In this case, the control of the converters allows to modify the power flow and relieve contingency-triggered overloads. Measuring the change of power flow in the AC-DC grid to changes of converter operating points, the power transfer compensation factor (PTCF) and the line

outage compensation factor (LOCF) are defined as follows:

$$PTCF_{\mathrm{AC},lk}=\frac{\Delta P_{\mathrm{AC},l}\big|_{\mathscr{B}_{\mathrm{AC}}\neq\emptyset}}{\Delta P_{\mathrm{DCAC},k}} \quad (28a) \qquad PTCF_{\mathrm{DC},lk}=\frac{\Delta P_{\mathrm{DC},l}\big|_{\mathscr{B}_{\mathrm{DC}}\neq\emptyset}}{\Delta P_{\mathrm{ACDC},k}} \quad (28b)$$

$$LOCF_{\mathrm{AC},lmk}=\frac{\Delta P_{\mathrm{AC},l}\big|_{m\in\mathscr{L}_{\mathrm{AC}}}}{\Delta P_{\mathrm{DCAC},k}} \quad (29a) \qquad LOCF_{\mathrm{DC},lmk}=\frac{\Delta P_{\mathrm{DC},l}\big|_{m\in\mathscr{L}_{\mathrm{DC}}}}{\Delta P_{\mathrm{ACDC},k}}. \quad (29b)$$

The PTCFs and LOCFs allow for the calculation of modified converter operating points for overload mitigation while considering outages of generators, loads, AC-DC converters, and lines. At first, the calculation of the PTCFs considering outages of generators, loads, and AC-DC converters is presented. Secondly, the calculation of the LOCFs is addressed. The calculation of the LOCFs is based on the concept of the compensated PTDF for AC grids [13].

1) Calculation of PTCF Considering Outages of Generators, Loads, and AC-DC Converters: Given the outage of a generator, a load, or an AC-DC converter connected to bus s, the altered power flows at initial converter operating points are specified by (24a) and (24b). When then adapting a converter operating point, power injections into the AC and DC grid parts are shifted, and the power flows in (24a) and (24b) are modified. Without loss of generality, the modification of the operating point of converter k connected to bus $\mathscr{z}$ is considered. The simultaneous change of further converter operating points to satisfy (15) is accounted for through superposition as performed in Section IV.

In contrast to (25a) and (25b), where the shifts of power injections due to a converter outage are specified by the initial converter power injections, the shifts of power injections due to a change of the converter operating points are variable. Thus, the shifts of power injections due to a change of converter operating points can be determined from a modified and more general form of (25a) and (25b):

$$\Delta P^{\mathrm{inj}}_{\mathrm{AC},\mathscr{z}} = c_{\mathrm{AC},\mathscr{z}k}\Delta P^{\mathrm{ctl}}_{\mathrm{DCAC},k} \quad (30a)$$

$$\Delta P^{\mathrm{inj}}_{\mathrm{DC},\mathscr{z}} = c_{\mathrm{DC},\mathscr{z}k}\Delta P^{\mathrm{ctl}}_{\mathrm{ACDC},k} \quad (30b)$$

where $\Delta P^{\mathrm{ctl}}_{\mathrm{DCAC},k}$ and $\Delta P^{\mathrm{ctl}}_{\mathrm{ACDC},k}$ are the changes of the power injections from the DC into the AC grid part and vice versa through converter k. As a consequence of the shifts of power injections in (30a) and (30b), the power flows at initial converter operating points $\widetilde{P}_{\mathrm{AC},l}$ and $\widetilde{P}_{\mathrm{DC},l}$ in (24a) and (24b) are modified by adding changes of flows $\Delta P^{\mathrm{ctl}}_{\mathrm{AC},l}$ and $\Delta P^{\mathrm{ctl}}_{\mathrm{DC},l}$:

$$\widetilde{P}^{\mathrm{ctl}}_{\mathrm{AC},l}\big|_{s\in\mathscr{B}_{\mathrm{AC}}} = P^{0}_{\mathrm{AC},l} + \Delta P^{\mathrm{ctl}}_{\mathrm{AC},l} + PTDF_{\mathrm{AC},ls}\Delta P^{\mathrm{inj}}_{\mathrm{AC},s} \quad (31a)$$

$$\widetilde{P}^{\mathrm{ctl}}_{\mathrm{DC},l}\big|_{s\in\mathscr{B}_{\mathrm{DC}}} = P^{0}_{\mathrm{DC},l} + \Delta P^{\mathrm{ctl}}_{\mathrm{DC},l} + PTDF_{\mathrm{DC},ls}\Delta P^{\mathrm{inj}}_{\mathrm{DC},s}. \quad (31b)$$

Since the changes of flows $\Delta P^{\mathrm{ctl}}_{\mathrm{AC},l}$ and $\Delta P^{\mathrm{ctl}}_{\mathrm{DC},l}$ result from the shifts of power injections $\Delta P^{\mathrm{inj}}_{\mathrm{AC},\mathscr{z}}$ and $\Delta P^{\mathrm{inj}}_{\mathrm{DC},\mathscr{z}}$ in the AC and DC grid parts, they can be specified taking into account the PTDFs for AC and DC grids introduced in Section III-A:

$$\Delta P^{\mathrm{ctl}}_{\mathrm{AC},l}\big|_{s\in\mathscr{B}_{\mathrm{AC}}} = PTDF_{\mathrm{AC},l\mathscr{z}}\Delta P^{\mathrm{inj}}_{\mathrm{AC},\mathscr{z}} \quad (32a)$$

$$\Delta P^{\mathrm{ctl}}_{\mathrm{DC},l}\big|_{s\in\mathscr{B}_{\mathrm{DC}}} = PTDF_{\mathrm{DC},l\mathscr{z}}\Delta P^{\mathrm{inj}}_{\mathrm{DC},\mathscr{z}}. \quad (32b)$$

Including (30a) and (30b) in (32a) and (32b) and inserting the result together with (24a) and (24b) into (31a) and (31b) yield the modified power flows considering the control of converter k:

$$\widetilde{P}^{\mathrm{ctl}}_{\mathrm{AC},l}\big|_{s\in\mathscr{B}_{\mathrm{AC}}} = \widetilde{P}_{\mathrm{AC},l}\big|_{s\in\mathscr{B}_{\mathrm{AC}}} + PTCF_{\mathrm{AC},lk}\Delta P^{\mathrm{ctl}}_{\mathrm{DCAC},k} \quad (33a)$$

$$\widetilde{P}^{\mathrm{ctl}}_{\mathrm{DC},l}\big|_{s\in\mathscr{B}_{\mathrm{DC}}} = \widetilde{P}_{\mathrm{DC},l}\big|_{s\in\mathscr{B}_{\mathrm{DC}}} + PTCF_{\mathrm{DC},lk}\Delta P^{\mathrm{ctl}}_{\mathrm{ACDC},k} \quad (33b)$$

where the newly introduced sensitivity factors $PTCF_{\mathrm{AC},lk}$ and $PTCF_{\mathrm{DC},lk}$ for congestion management considering outages of generators, loads, or AC-DC converters are specified by

$$PTCF_{\mathrm{AC},lk} = PTDF_{\mathrm{AC},l\mathscr{z}}c_{\mathrm{AC},\mathscr{z}k} \quad (34a)$$

$$PTCF_{\mathrm{DC},lk} = PTDF_{\mathrm{DC},l\mathscr{z}}c_{\mathrm{DC},\mathscr{z}k}. \quad (34b)$$

The calculations in (33a) and (33b) consist of two terms each. The first terms $\widetilde{P}_{\mathrm{AC},l}\big|_{s\in\mathscr{B}_{\mathrm{AC}}}$ and $\widetilde{P}_{\mathrm{DC},l}\big|_{s\in\mathscr{B}_{\mathrm{DC}}}$ denote the power flows over line l at initial AC-DC converter operating points while already considering the outage of a generator, a load, or an AC-DC converter connected to bus s. The second terms determine the changes of the power flows over line l when adapting the operating point of converter k. Thus, the newly introduced PTCFs in (34a) and (34b) facilitate the analysis of outages while taking into account the opportunity of changing converter operating points. This allows for the identification of modified converter operating points for overload mitigation.

From (20) and (21), it is possible to extend (34a) and (34b) for the case that the power injection of converter k at sending bus $\mathscr{z}$ is balanced by an opposite injection of converter h at bus $\mathscr{r}$:

$$PTCF_{\mathrm{AC},lkh} = PTDF_{\mathrm{AC},l\mathscr{z}\mathscr{r}}c_{\mathrm{AC},\mathscr{z}k}c_{\mathrm{AC},\mathscr{r}h} \quad (35a)$$

$$PTCF_{\mathrm{DC},lkh} = PTDF_{\mathrm{DC},l\mathscr{z}\mathscr{r}}c_{\mathrm{DC},\mathscr{z}k}c_{\mathrm{DC},\mathscr{r}h}. \quad (35b)$$

The multiplication of the coupling terms in the equations indicates that both must be equal to one for the power shifting to take place.

Based on the calculations of (33a) and (33b), equations for the specification of modified converter operating points for overload relief are derived later in Section IV-B.

2) Calculation of LOCF Considering Line Outages: Given the outage of a line m, the altered power flow at initial converter operating points is determined by (27a) and (27b). As in Section III-B1, it is again assumed that the operating point of converter k connected to bus $\mathscr{z}$ is modified and that further converter operating point changes to satisfy (15) are taken into account through superposition. When adapting the converter operating points, power injections are shifted as specified by (30a) and (30b), and the power flows of (27a) and (27b) are modified by adding changes of flows $\Delta P^{\mathrm{ctl}}_{\mathrm{AC},l}$, $\Delta P^{\mathrm{ctl}}_{\mathrm{AC},m}$, $\Delta P^{\mathrm{ctl}}_{\mathrm{DC},l}$, and $\Delta P^{\mathrm{ctl}}_{\mathrm{DC},m}$ to the initial flows $P^{0}_{\mathrm{AC},l}$, $P^{0}_{\mathrm{AC},m}$, $P^{0}_{\mathrm{DC},l}$, and $P^{0}_{\mathrm{DC},m}$, respectively:

$$\widetilde{P}^{\mathrm{ctl}}_{\mathrm{AC},l}\big|_{m\in\mathscr{L}_{\mathrm{AC}}}=(P^{0}_{\mathrm{AC},l}+\Delta P^{\mathrm{ctl}}_{\mathrm{AC},l})+LODF_{\mathrm{AC},lm}(P^{0}_{\mathrm{AC},m}+\Delta P^{\mathrm{ctl}}_{\mathrm{AC},m}) \quad (36a)$$

$$\widetilde{P}^{\mathrm{ctl}}_{\mathrm{DC},l}\big|_{m\in\mathscr{L}_{\mathrm{DC}}}=(P^{0}_{\mathrm{DC},l}+\Delta P^{\mathrm{ctl}}_{\mathrm{DC},l})+LODF_{\mathrm{DC},lm}(P^{0}_{\mathrm{DC},m}+\Delta P^{\mathrm{ctl}}_{\mathrm{DC},m}). \quad (36b)$$

Since the changes of flows $\Delta P^{\mathrm{ctl}}_{\mathrm{AC},l}$, $\Delta P^{\mathrm{ctl}}_{\mathrm{AC},m}$, $\Delta P^{\mathrm{ctl}}_{\mathrm{DC},l}$, and $\Delta P^{\mathrm{ctl}}_{\mathrm{DC},m}$ result from the shifts of power injections $\Delta P^{\mathrm{inj}}_{\mathrm{AC},\mathscr{z}}$ and $\Delta P^{\mathrm{inj}}_{\mathrm{DC},\mathscr{z}}$ of (32a) and (32b) the changes of flows can again be determined involving the developed PTDFs of Section III-A:

$$\widetilde{P}^{\mathrm{ctl}}_{\mathrm{AC},l}\big|_{m\in\mathscr{L}_{\mathrm{AC}}} = (P^{0}_{\mathrm{AC},l} + PTDF_{\mathrm{AC},l\mathscr{z}}\Delta P^{\mathrm{inj}}_{\mathrm{AC},\mathscr{z}}) + LODF_{\mathrm{AC},lm}(P^{0}_{\mathrm{AC},m} + PTDF_{\mathrm{AC},m\mathscr{z}}\Delta P^{\mathrm{inj}}_{\mathrm{AC},\mathscr{z}}) \quad (37a)$$

$$\widetilde{P}^{\mathrm{ctl}}_{\mathrm{DC},l}\big|_{m\in\mathscr{L}_{\mathrm{DC}}} = (P^{0}_{\mathrm{DC},l} + PTDF_{\mathrm{DC},l\mathscr{z}}\Delta P^{\mathrm{inj}}_{\mathrm{DC},\mathscr{z}}) + LODF_{\mathrm{DC},lm}(P^{0}_{\mathrm{DC},m} + PTDF_{\mathrm{DC},m\mathscr{z}}\Delta P^{\mathrm{inj}}_{\mathrm{DC},\mathscr{z}}). \quad (37b)$$

Inserting the shifts of power injections of (30a) and (30b) into (37a), (37b) yields the modified power flows considering the outage of line m and change of the operating point of

converter k:

$$\widetilde{P}^{\text{ctl}}_{\text{AC},l}\big|_{m\in\mathscr{L}_{\text{AC}}} = (P^{0}_{\text{AC},l} + PTDF_{\text{AC},l\mathfrak{z}}c_{\text{AC},\mathfrak{z}k}\Delta P^{\text{ctl}}_{\text{DCAC},k}) + LODF_{\text{AC},lm}(P^{0}_{\text{AC},m}+PTDF_{\text{AC},m\mathfrak{z}}c_{\text{AC},\mathfrak{z}k}\Delta P^{\text{ctl}}_{\text{DCAC},k}) \tag{38a}$$

$$\widetilde{P}^{\text{ctl}}_{\text{DC},l}\big|_{m\in\mathscr{L}_{\text{DC}}} = (P^{0}_{\text{DC},l} + PTDF_{\text{DC},l\mathfrak{z}}c_{\text{DC},\mathfrak{z}k}\Delta P^{\text{ctl}}_{\text{ACDC},k}) + LODF_{\text{DC},lm}(P^{0}_{\text{DC},m}+PTDF_{\text{DC},m\mathfrak{z}}c_{\text{DC},\mathfrak{z}k}\Delta P^{\text{ctl}}_{\text{ACDC},k}). \tag{38b}$$

The modified flows in (38a), (38b) are then rewritten by taking into account the altered power flows at initial converter operating points $\widetilde{P}_{\text{AC},l}$ and $\widetilde{P}_{\text{DC},l}$ of (27a), (27b)

$$\widetilde{P}^{\text{ctl}}_{\text{AC},l}\big|_{m\in\mathscr{L}_{\text{AC}}} = \widetilde{P}_{\text{AC},l}\big|_{m\in\mathscr{L}_{\text{AC}}} + LOCF_{\text{AC},lmk}\Delta P^{\text{ctl}}_{\text{DCAC},k} \tag{39a}$$

$$\widetilde{P}^{\text{ctl}}_{\text{DC},l}\big|_{m\in\mathscr{L}_{\text{DC}}} = \widetilde{P}_{\text{DC},l}\big|_{m\in\mathscr{L}_{\text{DC}}} + LOCF_{\text{DC},lmk}\Delta P^{\text{ctl}}_{\text{ACDC},k} \tag{39b}$$

where the respective newly introduced LOCFs for overload mitigation in AC-DC grids considering line outages are

$$LOCF_{\text{AC},lmk}=(PTDF_{\text{AC},l\mathfrak{z}}+LODF_{\text{AC},lm}PTDF_{\text{AC},m\mathfrak{z}})c_{\text{AC},\mathfrak{z}k} \tag{40a}$$

$$LOCF_{\text{DC},lmk}=(PTDF_{\text{DC},l\mathfrak{z}}+LODF_{\text{DC},lm}PTDF_{\text{DC},m\mathfrak{z}})c_{\text{DC},\mathfrak{z}k}. \tag{40b}$$

As for (33a) and (33b), the calculations in (39a) and (39b) also comprise two terms each. The first terms $\widetilde{P}_{\text{AC},l}\big|_{m\in\mathscr{L}_{\text{AC}}}$ and $\widetilde{P}_{\text{DC},l}\big|_{m\in\mathscr{L}_{\text{DC}}}$ denote the power flows over line l in the AC and DC grid parts at initial converter operating points while considering the outage of line m. The second terms specify the changes of the power flows over line l as a consequence of a change of the operating point of converter k. The LOCFs introduced in (40a) and (40b) facilitate the analysis of the AC-DC power flows considering line outages and converter operating point control.

As for the power transfer compensation factors in (35a) and (35b), it is also possible to model a direct power shifting from converter k at sending bus $\mathfrak{z}$ to converter h at receiving bus $\mathfrak{r}$ for the line outage compensation factors. Therefore, (40a) and (40b) are extended using (20) and (21):

$$LOCF_{\text{AC},lmkh}= =(PTDF_{\text{AC},l\mathfrak{z}\mathfrak{r}}+LODF_{\text{AC},lm}PTDF_{\text{AC},m\mathfrak{z}\mathfrak{r}})c_{\text{AC},\mathfrak{z}k}c_{\text{AC},\mathfrak{r}h} \tag{41a}$$

$$LOCF_{\text{DC},lmkh}= =(PTDF_{\text{DC},l\mathfrak{z}\mathfrak{r}}+LODF_{\text{DC},lm}PTDF_{\text{DC},m\mathfrak{z}\mathfrak{r}})c_{\text{DC},\mathfrak{z}k}c_{\text{DC},\mathfrak{r}h}. \tag{41b}$$

Based on the calculations of (39a) and (39b), modified AC-DC converter operating points for overload mitigation can be determined. Equations for this calculation are derived later in Section IV-B.

IV. Overload Mitigation using Compensation Factors

The linear sensitivity factors derived in Section III are now to be used for detection and mitigation of overloads in integrated AC-DC grids. For this purpose, Section IV culminates in the proposed algorithm for contingency analysis and overload mitigation in AC-DC grids. The algorithm benefits from the possibility to perform superposition of the effects of multiple changes of converter power injections on a line power flow by adding the respective sensitivity factors, as introduced in Section IV-A. Then, detailed equations and constraints for the calculation of modified converter operating points for overload mitigation using the introduced sensitivity factors are derived in Section IV-B. In Section IV-C, the overall proposed method for contingency analysis and overload mitigation is expressed through a flowchart.

A. Superposition of Linear Sensitivity Factors

The calculations in (33) and (39) specify the altered power flow over a line l in the AC and DC grid parts while taking into account the outage of a generator, a load, an AC-DC converter, or a line as well as the change of the operating point of converter k. However, multiple outages and changes of multiple converter operating points may also be considered. Since the presented sensitivity factors for overload detection and mitigation are linear, the effects of multiple outages and changes of multiple converter operating points on the power flow can be calculated using superposition. The power flow of an AC-DC grid considering multiple outages and changes of multiple converter operating points can be represented in matrix form as follows:

$$\widetilde{\boldsymbol{P}}^{\text{ctl}}_{\text{AC}} = \widetilde{\boldsymbol{P}}_{\text{AC}} + \boldsymbol{CCM}_{\text{AC}}\Delta\boldsymbol{P}^{\text{ctl}}_{\text{DCAC}} \tag{42a}$$

$$\widetilde{\boldsymbol{P}}^{\text{ctl}}_{\text{DC}} = \widetilde{\boldsymbol{P}}_{\text{DC}} + \boldsymbol{CCM}_{\text{DC}}\Delta\boldsymbol{P}^{\text{ctl}}_{\text{ACDC}} \tag{42b}$$

where entries of the vectors $\widetilde{\boldsymbol{P}}_{\text{AC}} \in \mathbb{R}^{n_{\text{l,AC}}}$ and $\widetilde{\boldsymbol{P}}_{\text{DC}} \in \mathbb{R}^{n_{\text{l,DC}}}$ are line power flows at initial converter operating points considering multiple outages of generators, loads, AC-DC converters, and lines; $n_{\text{l,AC}}$ and $n_{\text{l,DC}}$ are the number of AC and DC lines, respectively; entries of the vectors $\Delta\boldsymbol{P}^{\text{ctl}}_{\text{DCAC}} \in \mathbb{R}^{n_{\text{conv}}}$ and $\Delta\boldsymbol{P}^{\text{ctl}}_{\text{ACDC}} \in \mathbb{R}^{n_{\text{conv}}}$ are the changes of power injections from the DC into the AC grid parts and vice versa through the converters; $\boldsymbol{CCM}_{\text{AC}} \in \mathbb{R}^{n_{\text{l,AC}}\times n_{\text{conv}}}$ and $\boldsymbol{CCM}_{\text{DC}} \in \mathbb{R}^{n_{\text{l,DC}}\times n_{\text{conv}}}$ are the newly introduced congestion compensation matrices, whose entries are specified by addition of the PTCFs of (34a) and (34b) and LOCFs of (40a) and (40b) for AC and DC grid parts, respectively, to allow for superposition of the effects of multiple changes of converter power injections on a line power flow; entry lk of $\boldsymbol{CCM}_{\text{AC}}$ and $\boldsymbol{CCM}_{\text{DC}}$ measures the respective change of flow over line l in the AC and DC grid parts to a change of the operating point of converter k. The calculations of (42) allow for a unified analysis of the AC-DC power flows considering multiple outages of generators, loads, converters, or lines while taking into account the opportunity of modifying multiple converter operating points.

B. Calculation of New Converter Operating Points for Overload Mitigation

Overloads on lines can be mitigated if it is possible to transmit the excessive power over alternative lines of the grid. Given the power flow calculations of (42a) and (42b), and considering the limits of power injections of AC-DC converters, an inequality system can be defined as follows:

$$\begin{bmatrix} -\boldsymbol{P}^{\text{lim}}_{\text{AC}} \\ -\boldsymbol{P}^{\text{lim}}_{\text{DC}} \\ -\boldsymbol{P}^{\text{lim}}_{\text{DCAC}} \\ -\boldsymbol{P}^{\text{lim}}_{\text{ACDC}} \end{bmatrix} \preceq \begin{bmatrix} \widetilde{\boldsymbol{P}}_{\text{AC}} + \boldsymbol{CCM}_{\text{AC}}\Delta\boldsymbol{P}^{\text{ctl}}_{\text{DCAC}} \\ \widetilde{\boldsymbol{P}}_{\text{DC}} + \boldsymbol{CCM}_{\text{DC}}\Delta\boldsymbol{P}^{\text{ctl}}_{\text{ACDC}} \\ \boldsymbol{P}^{0}_{\text{DCAC}} + \Delta\boldsymbol{P}^{\text{ctl}}_{\text{DCAC}} \\ \boldsymbol{P}^{0}_{\text{ACDC}} + \Delta\boldsymbol{P}^{\text{ctl}}_{\text{ACDC}} \end{bmatrix} \preceq \begin{bmatrix} \boldsymbol{P}^{\text{lim}}_{\text{AC}} \\ \boldsymbol{P}^{\text{lim}}_{\text{DC}} \\ \boldsymbol{P}^{\text{lim}}_{\text{DCAC}} \\ \boldsymbol{P}^{\text{lim}}_{\text{ACDC}} \end{bmatrix} \tag{43}$$

where $\preceq$ denotes elementwise smaller or equal; entries of $\boldsymbol{P}^{0}_{\text{DCAC}}$ and $\boldsymbol{P}^{0}_{\text{ACDC}}$ are the initial converter power injections from the DC into the AC grid parts and vice versa; entries of $\boldsymbol{P}^{\text{lim}}_{\text{AC}}$ and $\boldsymbol{P}^{\text{lim}}_{\text{DC}}$ are the transfer capacities of AC and DC lines; entries of $\boldsymbol{P}^{\text{lim}}_{\text{ACDC}}$ and $\boldsymbol{P}^{\text{lim}}_{\text{DCAC}}$ are the limits of the real power injections of AC-DC converters. The changes of converter power injections

$\Delta \boldsymbol{P}^{\text{ctl}}_{\text{DCAC}}$ and $\Delta \boldsymbol{P}^{\text{ctl}}_{\text{ACDC}}$ are related by the power equality constraints of (13) and (15). Neglecting converter losses, those power equality constraints are rewritten in matrix form as

$$\Delta \boldsymbol{P}^{\text{ctl}}_{\text{DCAC}} + \Delta \boldsymbol{P}^{\text{ctl}}_{\text{ACDC}} = \boldsymbol{0} \quad (44) \qquad \boldsymbol{\sigma}^{\top}_{1\times n_{\text{conv}}} \Delta \boldsymbol{P}^{\text{ctl}}_{\text{ACDC}} = 0 \quad (45)$$

where $\boldsymbol{\sigma}^{\top}_{1\times n_{\text{conv}}}$ is a vector of ones of dimension $1 \times n_{\text{conv}}$:

$$\boldsymbol{\sigma}^{\top}_{1\times n_{\text{conv}}} = [1, \ldots, 1]. \quad (46)$$

To enable a unified analysis of the inequality system of (43) and the equality constraints of (44) and (45), the equations are combined and rewritten into the standard form $\boldsymbol{A}\boldsymbol{x} \preceq \boldsymbol{b}$. Therefore, the two inequality systems of (43) are reformulated as

$$\begin{bmatrix} \boldsymbol{CCM}_{\text{AC}} & \boldsymbol{0}_{n_{\text{conv}}} \\ \boldsymbol{0}_{n_{\text{conv}}} & \boldsymbol{CCM}_{\text{DC}} \\ \boldsymbol{I}_{n_{\text{conv}}} & \boldsymbol{0}_{n_{\text{conv}}} \\ \boldsymbol{0}_{n_{\text{conv}}} & \boldsymbol{I}_{n_{\text{conv}}} \\ \boldsymbol{I}_{n_{\text{conv}}} & \boldsymbol{I}_{n_{\text{conv}}} \\ \boldsymbol{0}_{1\times n_{\text{conv}}} & \boldsymbol{\sigma}^{\top}_{1\times n_{\text{conv}}} \end{bmatrix} \begin{bmatrix} \Delta \boldsymbol{P}^{\text{ctl}}_{\text{DCAC}} \\ \Delta \boldsymbol{P}^{\text{ctl}}_{\text{ACDC}} \end{bmatrix} \succeq \begin{bmatrix} -\boldsymbol{P}^{\text{lim}}_{\text{AC}} - \widetilde{\boldsymbol{P}}_{\text{AC}} \\ -\boldsymbol{P}^{\text{lim}}_{\text{DC}} - \widetilde{\boldsymbol{P}}_{\text{DC}} \\ -\boldsymbol{P}^{\text{lim}}_{\text{DCAC}} - \boldsymbol{P}^{0}_{\text{DCAC}} \\ -\boldsymbol{P}^{\text{lim}}_{\text{ACDC}} - \boldsymbol{P}^{0}_{\text{ACDC}} \\ \boldsymbol{0} \\ 0 \end{bmatrix} \quad (47)$$

$$\begin{bmatrix} \boldsymbol{CCM}_{\text{AC}} & \boldsymbol{0}_{n_{\text{conv}}} \\ \boldsymbol{0}_{n_{\text{conv}}} & \boldsymbol{CCM}_{\text{DC}} \\ \boldsymbol{I}_{n_{\text{conv}}} & \boldsymbol{0}_{n_{\text{conv}}} \\ \boldsymbol{0}_{n_{\text{conv}}} & \boldsymbol{I}_{n_{\text{conv}}} \\ \boldsymbol{I}_{n_{\text{conv}}} & \boldsymbol{I}_{n_{\text{conv}}} \\ \boldsymbol{0}_{1\times n_{\text{conv}}} & \boldsymbol{\sigma}^{\top}_{1\times n_{\text{conv}}} \end{bmatrix} \begin{bmatrix} \Delta \boldsymbol{P}^{\text{ctl}}_{\text{DCAC}} \\ \Delta \boldsymbol{P}^{\text{ctl}}_{\text{ACDC}} \end{bmatrix} \preceq \begin{bmatrix} \boldsymbol{P}^{\text{lim}}_{\text{AC}} - \widetilde{\boldsymbol{P}}_{\text{AC}} \\ \boldsymbol{P}^{\text{lim}}_{\text{DC}} - \widetilde{\boldsymbol{P}}_{\text{DC}} \\ \boldsymbol{P}^{\text{lim}}_{\text{DCAC}} - \boldsymbol{P}^{0}_{\text{DCAC}} \\ \boldsymbol{P}^{\text{lim}}_{\text{ACDC}} - \boldsymbol{P}^{0}_{\text{ACDC}} \\ \boldsymbol{0} \\ 0 \end{bmatrix} \quad (48)$$

where $\succeq$ denotes elementwise larger or equal; $\boldsymbol{I}_{n_{\text{conv}}}$ is an identity matrix of dimension $n_{\text{conv}} \times n_{\text{conv}}$; $\boldsymbol{0}_{n_{\text{conv}}}$ is a zero matrix of dimension $n_{\text{conv}} \times n_{\text{conv}}$; $\boldsymbol{0}_{1\times n_{\text{conv}}}$ is a zero matrix of dimension $1 \times n_{\text{conv}}$. The inequality system of (47) is multiplied by -1 and combined again with inequality system (48), leading to

$$\boldsymbol{CCM} \begin{bmatrix} \Delta \boldsymbol{P}^{\text{ctl}}_{\text{DCAC}} \\ \Delta \boldsymbol{P}^{\text{ctl}}_{\text{ACDC}} \end{bmatrix} \preceq \Delta \boldsymbol{P}^{\text{lim}} \quad (49)$$

where $\boldsymbol{CCM}$ and $\Delta \boldsymbol{P}^{\text{lim}}$ are defined in (50) and (51).

Congestion management through adaptation of converter operating points is possible if the inequality system of (49) has a feasible solution. Feasible solutions can be determined by applying an interior-point method to the inequality system [29]. Given a feasible solution of (49), new VSC operating points for overload mitigation are specified.

$$\boldsymbol{CCM} = \begin{bmatrix} -\boldsymbol{CCM}_{\text{AC}} & \boldsymbol{0}_{n_{\text{conv}}} \\ \boldsymbol{0}_{n_{\text{conv}}} & -\boldsymbol{CCM}_{\text{DC}} \\ -\boldsymbol{I}_{n_{\text{conv}}} & \boldsymbol{0}_{n_{\text{conv}}} \\ \boldsymbol{0}_{n_{\text{conv}}} & -\boldsymbol{I}_{n_{\text{conv}}} \\ -\boldsymbol{I}_{n_{\text{conv}}} & -\boldsymbol{I}_{n_{\text{conv}}} \\ \boldsymbol{0}_{1\times n_{\text{conv}}} & -\boldsymbol{\sigma}^{\top}_{1\times n_{\text{conv}}} \\ \boldsymbol{CCM}_{\text{AC}} & \boldsymbol{0}_{n_{\text{conv}}} \\ \boldsymbol{0}_{n_{\text{conv}}} & \boldsymbol{CCM}_{\text{DC}} \\ \boldsymbol{I}_{n_{\text{conv}}} & \boldsymbol{0}_{n_{\text{conv}}} \\ \boldsymbol{0}_{n_{\text{conv}}} & \boldsymbol{I}_{n_{\text{conv}}} \\ \boldsymbol{I}_{n_{\text{conv}}} & \boldsymbol{I}_{n_{\text{conv}}} \\ \boldsymbol{0}_{1\times n_{\text{conv}}} & \boldsymbol{\sigma}^{\top}_{1\times n_{\text{conv}}} \end{bmatrix} \quad (50)$$

$$\Delta \boldsymbol{P}^{\text{lim}} = \begin{bmatrix} \boldsymbol{P}^{\text{lim}}_{\text{AC}} + \widetilde{\boldsymbol{P}}_{\text{AC}} \\ \boldsymbol{P}^{\text{lim}}_{\text{DC}} + \widetilde{\boldsymbol{P}}_{\text{DC}} \\ \boldsymbol{P}^{\text{lim}}_{\text{DCAC}} + \boldsymbol{P}^{0}_{\text{DCAC}} \\ \boldsymbol{P}^{\text{lim}}_{\text{ACDC}} + \boldsymbol{P}^{0}_{\text{ACDC}} \\ \boldsymbol{0} \\ 0 \\ \boldsymbol{P}^{\text{lim}}_{\text{AC}} - \widetilde{\boldsymbol{P}}_{\text{AC}} \\ \boldsymbol{P}^{\text{lim}}_{\text{DC}} - \widetilde{\boldsymbol{P}}_{\text{DC}} \\ \boldsymbol{P}^{\text{lim}}_{\text{DCAC}} - \boldsymbol{P}^{0}_{\text{DCAC}} \\ \boldsymbol{P}^{\text{lim}}_{\text{ACDC}} - \boldsymbol{P}^{0}_{\text{ACDC}} \\ \boldsymbol{0} \\ 0 \end{bmatrix} \quad (51)$$

C. Flowchart of Process

Based on the foundations established in Section III-A to Section IV-B, a process for contingency analysis and overload compensation was developed and formulated in the flowchart of Fig. 1. After importing the grid data and initializing the outage counter ν, sensitivity factors PTDF and LODF of the AC and DC grid parts are calculated. The altered AC-DC power flow is specified considering an outage of a generator, a load, a converter, or a line. Overloads are detected by analyzing if the power flow exceeds the transfer capacity of the line.

If overloads are detected, the outage scenario is saved, and $\boldsymbol{CCM}$ as well as $\Delta \boldsymbol{P}^{\text{lim}}$ of inequality system (49) are calculated using (50) and (51), respectively. Depending on the considered outage, the entries of $\boldsymbol{CCM}$ are determined by using (34a) and (34b) or (40a) and (40b). The entries of $\Delta \boldsymbol{P}^{\text{lim}}$ are specified by using the limits of real power transfers and by (24a) and (24b) or (27a) and (27b).

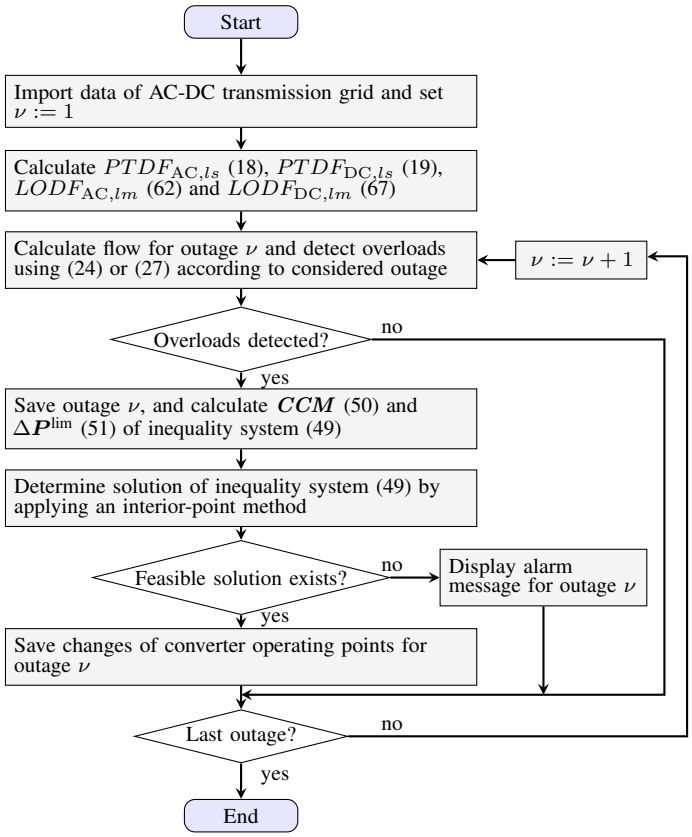

Fig. 1. Flowchart of contingency analysis and overload mitigation based on linear sensitivity methods.

Overloads can be relieved by adapting converter operating points if the inequality system of (49) has a feasible solution. A solution of (49) can be determined by applying an interior-point method. If a feasible solution exists, then the new converter operating points for overload mitigation are saved.

If there is no feasible solution, then an alarm message is displayed [13]. The alarm message indicates that the considered outage would lead to congestion of transmission lines and that the congestion cannot be relieved by modifying AC-DC converter operating points.

To deal with situations in which the modification of AC-DC converter operating points does not yield a solution, the process may be extended. In this context, security-constrained optimal power flow (SCOPF) calculation as a function of system security may be applied to determine appropriate redispatch measures.

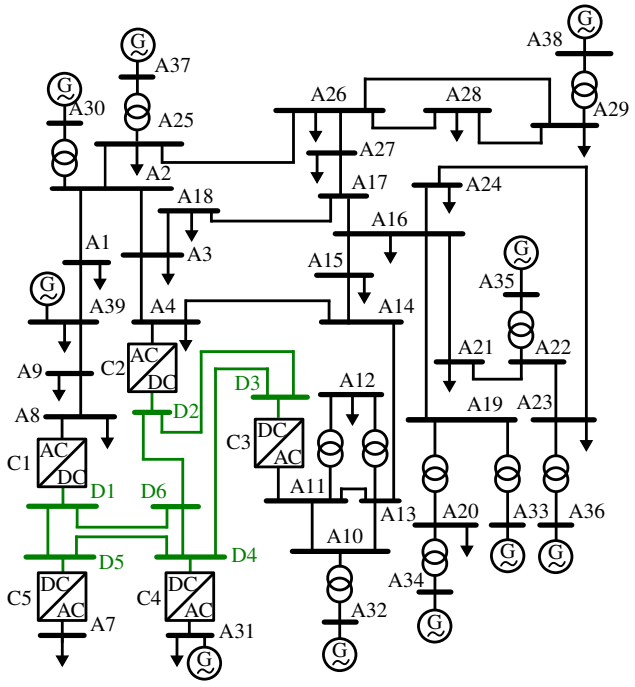

Fig. 2. Modified version of the IEEE AC-DC 39+6-bus system [30].

V. Validation

The performance indicators considered here are the functionality, accuracy, and robustness. The validation of the proposed method comprises three stages. In Section V-A, the process of overload detection is addressed. The functionality in terms of detected overloads and the accuracy of the power flow calculation based on linear sensitivity factors compared to the nonlinear power flow calculation are analyzed. In Section V-B, the assessment of functionality and accuracy is extended towards the novel compensation factors and their application for overload mitigation. In the third stage in Section V-C, the robustness of the method towards parameter uncertainty is addressed. The robustness is tested by analyzing the impact of stochastic variations in network parameters on the linear sensitivity factors.

The considered test system is the IEEE 39-bus system augmented with five-terminal DC grid as depicted in Fig. 2 and modified from [30], [31]. The dataset of this AC-DC 39+6-bus system is included in Appendix C. All program code was implemented in Matlab R2020b and executed on a personal computer with a processor Intel(R) Core(TM) i7-7700K and 32 GB RAM.

A. Overload Detection

In what follows, the functionality and accuracy of the overload detection process is evaluated. First, the results of the proposed AC-DC contingency analysis and overload detection are demonstrated. Then, the accuracy of these results is verified. For this purpose, the relative deviation in branch power flows and currents calculated with the proposed linear AC-DC power flow calculus and a nonlinear AC-DC power flow calculus as in [32] is assessed.

The rated power of each AC-DC converter is $1000\,\mathrm{MVA}$. The initial power exchanges from DC to AC grid parts are specified for converters C1 to C4, while converter C5 ensures power balance, which is accomplished using (14) in the linear power flow calculation:

$$\boldsymbol{P}^{0}_{\mathrm{DCAC}} = \begin{bmatrix} 760.8 & 558.5 & -562.3 & -990.8 & 233.8 \end{bmatrix}^{\top} \mathrm{MW} \tag{52}$$

According to Fig. 1, single outages of AC transmission lines, AC generators, and DC transmission lines were considered. For each possible scenario, the power flows were calculated by (24) or (27), respectively. The power flows were then compared with the limits of real power flows specified in Table VI, Table VII, and Table VIII of Appendix C. Overloads were detected in 26 scenarios, as listed in Table I.

To verify the accuracy of the proposed method, an outage in the DC grid part was considered, and line D2-D6 was taken as an example. The results of the linear and nonlinear power flow calculations for the real power flows are shown in Table II. The corresponding results for the root-mean-square (RMS) values of the currents in the AC grid part as well as the magnitudes of the currents in the DC grid part are considered in Table III.

Since the method's scope is centered on the evaluation of highly loaded or overloaded lines, only branches with a loading of at least $70\,\%$ are considered. In Table II, the maximum of the magnitudes of the relative deviations between the results of the linear and nonlinear power flow calculations is $2.4\,\%$. The results are in accordance with the accuracy of linear power flow calculation of AC transmission grids, given at around 5 % [13]. Since the linear power flow calculus is primarily formulated for the computation of real power flows, the results for the latter are generally more accurate than for current flows. This is also observed in Table III, where the recorded results for AC RMS values and DC magnitudes reveal magnitudes of deviations of up to $4\,\%$, respectively. Both lower and higher deviations were observed for other contingencies. Thus, for the detection of the violation of a flow limit, a margin should be considered to adjust for the relative deviation compared with nonlinear power flow calculus. In this context, it is recommended to modify the actual flow limit by 10 % for the purpose of detecting overloads based on linear calculations. Then, the accuracies are such that both power flows or current flows may serve as a basis for comparisons regarding branch flow limits. In the flowchart of Fig. 1, limits for real power flows are considered.

In accordance with the made assumption that AC voltage magnitudes are at 1 p.u., linear power flow calculus is as such not suitable to evaluate voltage magnitudes in AC grids [13]. The results obtained in the context of this validation confirm that the assumption is plausible. During all studies of normal operation and contingencies performed for the AC-DC 39+6-bus system in Fig. 2, there was only one contingency where the magnitude of the voltage of a single bus fell out of the range from 0.9 p.u. to 1.1 p.u., which is the acceptable range as specified by the European Network of Transmission System Operators for Electricity (ENTSO-E) [33]. This specific voltage drop occurred at bus A15 during the outage of transmission line A15-A16. During this outage, bus A15 is connected to the remaining part of the AC-DC system by just one other transmission line A14-A15. Also, bus A15 is a bus with a relatively high load in terms of both active and reactive power, and the bus is not directly linked to any bus with controlled voltage close by. When such or similar situations are observed, the nonlinear power flow calculus provides a basis for further analysis of the AC voltages.

TABLE I
OUTAGE SCENARIOS WITH CONTINGENCY-TRIGGERED OVERLOADS AND IDENTIFICATION IF OVERLOADS CAN BE MITIGATED

Outage of generators		Outage of AC lines		Outage of DC lines	
Bus connection	Overloads can be mitigated	Bus connection	Overloads can be mitigated	Bus connection	Overloads can be mitigated
A32	yes	A2-A3	yes	D1-D6	yes
A33	yes	A2-A25	yes	D2-D3	no
A34	yes	A3-A18	yes	D2-D6	yes
A35	yes	A4-A14	yes	D3-D4	no
A36	yes	A10-A11	no	D4-D6	yes
A39	yes	A10-A13	no	D4-D5	yes
-	-	A14-A15	yes	-	-
-	-	A16-A17	yes	-	-
-	-	A16-A21	no	-	-
-	-	A17-A18	yes	-	-
-	-	A17-A27	yes	-	-
-	-	A21-A22	no	-	-
-	-	A23-A24	no	-	-
-	-	A26-A27	no	-	-

B. Overload Mitigation

Having confirmed the functionality and accuracy of the method for overload detection, a similar assessment is conducted for the proposed overload mitigation. For each outage scenario in which too high a real power flow over a branch was detected, the converter operating points were optimized by solving (49). As indicated in Table I, in 18 out of 26 scenarios a feasible solution was found, so that the overload can be mitigated. The results of the proposed method were also confirmed by nonlinear power flow analysis that was performed for comparison. For the cases where overloads could not be relieved by just controlling converter operating points, the results were reconfirmed by an exhaustive search.

The optimization of converter operating points to mitigate overloads is based on the novel compensation factors. The accuracy of the power flow calculation using these factors was evaluated again taking the nonlinear power flow calculation as a reference. For the sake of illustration, the results for one outage scenario, the outage of line D2-D6, are presented in detail. At the initial converter operating points (52), the line D2-D3 was overloaded, for example. After solving the optimization problem (49), the following adjusted converter operating points given in MW were found:

$$\boldsymbol{P}_{\mathrm{DCAC}}^{\mathrm{ctl}} = \begin{bmatrix} 760.8 & 480.0 & -575.0 & -899.6 & 233.8 \end{bmatrix}^{\top}. \quad (53)$$

The optimization of the AC-DC converter operating points led to modified branch power flows as shown in Table IV for linear and nonlinear power flow calculus. As given in the last row of this table, the absolute value of the power flow over the line D2-D3 is decreased, such that the power flow does not violate the limit. This result confirms the functionality of the proposed optimization method for overload mitigation.

For the considered outage, the magnitudes of the relative deviations between the results of the linear and nonlinear power flow calculations are listed in Table IV. In general, the observations resulting from the analysis of the accuracy of the deviations made in Section V-A also apply to overload mitigation.

C. Robustness Towards Parameter Uncertainty

When calculating linear sensitivity factors, the grid parameters, such as admittances of transmission lines, are typically considered as given. In reality, however, those parameters are subject to a certain degree of uncertainty. For evaluating the robustness of the developed method, the impact of parameter uncertainty on the linear sensitivity factors is analyzed using Monte-Carlo simulation as a stochastic method.

TABLE II
REAL POWER FLOWS OVER BRANCHES WITH AT LEAST 70 % LOADING AT INITIAL CONVERTER OPERATING POINTS AND OUTAGE OF LINE D2-D6

Bus connection	Power in nonlinear calculation [MW]	Power in linear calculation [MW]	Relative deviation [%]
A4-A14	−475.36	−486.71	2.39
A10-A11	584.13	584.79	0.11
A10-A13	584.50	585.21	0.12
A10-A32	−1170.00	−1170.00	0.00
A13-A14	594.74	599.17	0.74
A16-A19	−472.45	−480.00	1.60
A19-A33	−640.49	−642.00	0.24
A22-A35	−660.00	−660.00	0.00
D2-D3	−569.19	−558.50	−1.88

TABLE III
CURRENT FLOWS OVER BRANCHES WITH AT LEAST 70 % LOADING AT INITIAL CONVERTER OPERATING POINTS AND OUTAGE OF LINE D2-D6

Bus connection	RMS current in nonlinear calculation [A]	RMS current in linear calculation [A]	Relative deviation [%]
A4-A14	803.71	814.50	1.34
A10-A11	980.93	978.63	−0.23
A10-A13	981.51	979.34	−0.22
A10-A32	2030.37	1957.97	−3.57
A13-A14	1001.61	1002.70	0.11
A16-A19	772.89	803.27	3.93
A19-A33	1062.14	1074.37	1.15
A22-A35	1101.97	1104.50	0.23
D2-D3	887.23	865.89	−2.41

For each AC and DC branch admittance, a normal distribution with the mean equal to the admittance given in the grid data set and the standard deviation equal to 10 % of the admittance was considered. Then, the Power Transfer Distribution Factors were calculated according to (18) and (19), whereas each branch admittance was randomly sampled from the corresponding normal distribution. In accordance with guidelines from [34], 7500 samples were taken. As such, a set of 7500 values was obtained for $PTDF_{\mathrm{AC},ls}$ and $PTDF_{\mathrm{DC},ls}$. The mean of the 7500 $PTDF_{\mathrm{AC},ls}$ and $PTDF_{\mathrm{DC},ls}$ for each s and l generated in the stochastic process was eventually compared to the values of the $PTDF_{\mathrm{AC},ls}$ and $PTDF_{\mathrm{DC},ls}$ calculated with given admittances without parameter uncertainty. The same process was applied to the other linear sensitivity factors: LODF, PTCF, and LOCF.

The second and third columns of Table V give the maximal magnitudes of the absolute and relative deviations between the values of each linear sensitivity factor obtained with and without considering the parameter uncertainty, respectively. To calculate a relative deviation with respect to a value of a linear sensitivity factor calculated without parameter uncertainty, a deviation with an absolute value smaller than 10^{-12} was rounded to 0. In all cases considered, the relative deviations remained lower than 1 %.

To further examine the extent to which parameter uncertainty affects the linear sensitivity factors, the analysis was repeated with a larger range of uncertainty. For each AC and DC branch admittance, 7500 samples from a normal distribution with the mean equal to the admittance given by the grid data and the standard deviation equal to 25 % of the admittance were taken. Then, the same approach was conducted to calculate the deviations in PTDF, LODF, PTCF, and LOCF values

TABLE IV
REAL POWER FLOWS OVER BRANCHES WITH AT LEAST 70 % LOADING AT OPTIMIZED CONVERTER OPERATING POINTS AND OUTAGE OF LINE D2-D6

Bus connection	Power in nonlinear calculation [MW]	Power in linear calculation [MW]	Relative deviation [%]
A4-A14	−488.81	−500.00	2.29
A10-A11	584.27	584.93	0.11
A10-A13	584.35	585.07	0.12
A10-A32	−1170.00	−1170.00	0.00
A13-A14	582.12	586.48	0.75
A16-A19	−472.45	−480.00	1.60
A19-A33	−640.49	−642.00	0.24
A22-A35	−660.00	−660.00	0.00
D2-D3	−487.77	−480.00	−1.59

TABLE V
MAXIMAL MAGNITUDES OF DEVIATION BETWEEN VALUES OF SENSITIVITY FACTORS OBTAINED WITH AND WITHOUT PARAMETER UNCERTAINTY

Factor	Standard deviation in admittance equal to 10 % of given admittance		Standard deviation in admittance equal to 25 % of given admittance	
	Absolute deviation	Relative deviation	Absolute deviation	Relative deviation
$PTDF_{\mathrm{AC}}$	$7.39 \cdot 10^{-4}$	0.56 %	$5.38 \cdot 10^{-3}$	4.45 %
$LODF_{\mathrm{AC}}$	$3.01 \cdot 10^{-4}$	0.56 %	$3.12 \cdot 10^{-3}$	4.66 %
$PTCF_{\mathrm{AC}}$	$1.82 \cdot 10^{-4}$	0.56 %	$2.39 \cdot 10^{-3}$	4.45 %
$LOCF_{\mathrm{AC}}$	$3.01 \cdot 10^{-4}$	0.56 %	$3.12 \cdot 10^{-3}$	4.66 %
$PTDF_{\mathrm{DC}}$	$6.40 \cdot 10^{-4}$	0.47 %	$2.04 \cdot 10^{-3}$	2.84 %
$LODF_{\mathrm{DC}}$	$2.75 \cdot 10^{-4}$	0.22 %	$2.10 \cdot 10^{-3}$	2.69 %
$PTCF_{\mathrm{DC}}$	$6.40 \cdot 10^{-4}$	0.47 %	$2.04 \cdot 10^{-3}$	2.84 %
$LOCF_{\mathrm{DC}}$	$6.23 \cdot 10^{-4}$	0.26 %	$2.84 \cdot 10^{-3}$	2.69 %

obtained with and without considering parameter uncertainty. The maximal magnitudes of the absolute and relative deviations under these conditions are listed in the fourth and fifth columns of Table V. As the relative deviations do not exceed 5 %, the simulation results confirm that the method remains accurate even if the network parameters are subject to significant uncertainties.

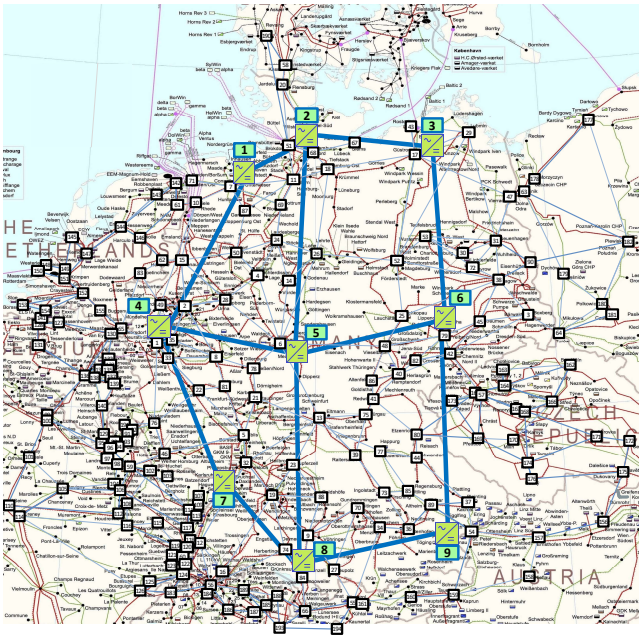

Fig. 3. Schematic model of hypothetical future DC overlay grid in Germany.

VI. APPLICATION

In the following, the benefits in terms of reduced computational effort when using the developed linear contingency analysis and control are confirmed by applying the method for a realistic large-scale integrated AC-DC grid. The test system represents a hypothetical scenario of the future German transmission system and is characterized by high wind power generation in the northern part of the country, while several important load centers are located in the southern part. Thus, power transport over long distances is necessary, and the multi-terminal overlay DC grid depicted in Fig. 3 is introduced [2].

The DC grid consists of nine AC-DC converter stations with a maximal capacity of 6 GVA, and twelve DC transmission corridors arranged in north-south corridors with the capacity of 10 GW and east-west corridors with the capacity of 5 GW. The AC grid model comprises 194 buses, 75 generators, and 398 transmission lines. The conducted case study considered single outages of generators as well as of AC and DC transmission lines. In total, 485 scenarios were evaluated.

For all scenarios, the algorithm of Fig. 1 is used. Regarding the outages of AC generators, in 42 out of 75 cases an overload was detected, yet in 41 cases it could be mitigated by the contingency control through optimization of the converter operating points. Regarding the AC transmission line outages, overloads occurred in 180 out of 398 scenarios, subsequent overload reliefs were achieved in 164 cases. Finally, outages in the DC grid part led to three identified overloads, out of which one was alleviated after the optimization of converter operating points. The results are visualized in Fig. 4. While overloads were detected in a substantial share of scenarios, thanks to the developed optimized control of AC-DC converters 91.6 % of them could be mitigated. As such, a secure operation of the system could be maintained after 466 out of 485 possible outages.

Using Matlab R2020b and the personal computer mentioned in Section V, the whole process took around 20 seconds. A nonlinear power flow calculation considering single AC line outages, single AC generator outages, and single DC line outages was also conducted. It took around 92 minutes. This outcome proves the applicability and the practical benefits of the proposed linear contingency analysis for realistic large-scale AC-DC power systems.

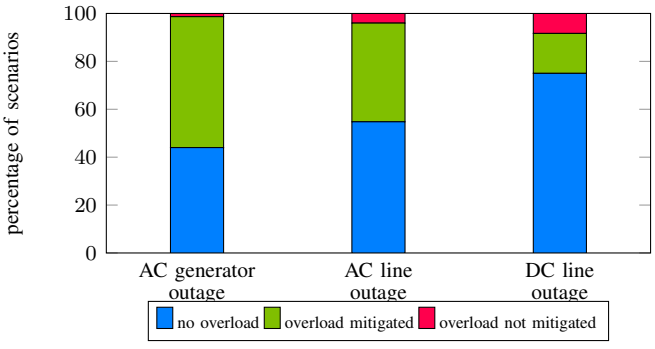

Fig. 4. Evaluation of effectiveness of overload mitigation in large test system.

VII. CONCLUSION

A methodology for fast contingency analysis and control of integrated AC-DC transmission grids was developed. Inspired by the contingency analysis of AC transmission grids, the

proposed contingency analysis and control of integrated AC-DC transmission grids is also based on linear sensitivity methods, allowing for the efficient evaluation of a large number of scenarios. To readily address contingency-triggered overloads, the newly developed algorithm enables the mitigation of the detected overloads by making use of the power flow control capability of the AC-DC voltage sourced converters without referring to a redispatch of power generation.

As part of the development, three key contributions were made. First, sensitivity factors as known from contingency analysis of AC power transmission systems were redeveloped for the analysis of integrated AC-DC grids. An important role is attributed to the line outage compensation factor LOCF. This factor gives the sensitivity measuring a change of power flow on the studied line to a change of power injection by an AC-DC converter while there is a simultaneous outage of another specified line. The factor is formulated in two variants depending on its application for AC or DC grid parts.

Second, a method of line overload mitigation was developed to integrate congestion management with the contingency analysis of AC-DC grids. This contingency control makes use of the sensitivity factors and an interior point method to optimize the operating points of the AC-DC voltage sourced converters. The objective of the optimization is to reach a system-wide overload relief of lines during a contingency. Third, the claims were substantiated through validation and application studies, covering accuracy, robustness, and efficiency. Those studies covered the IEEE 39-bus system augmented with a five-terminal DC grid, and a large-scale AC grid model of Germany with an integrated overlay DC grid. The contingency analysis and control functions demonstrated a high level of accuracy. All contingencies were shown to be detected. In the thorough accuracy analysis based on the modified IEEE AC-DC 39+6-bus system, magnitudes of relative deviations in power flows of heavily loaded branches between the proposed linear and the nonlinear solution were in the same range that is observed when AC grids alone are considered. Impressive was also the robustness of the proposed sensitivity factors toward parameter uncertainty. For standard deviations of all branch admittances as large as 25 %, the changes of the power transfer distribution factors did not exceed 5 % for both AC and DC grid parts, respectively.

For a large-scale future AC-DC grid covering Germany, the contingency analysis and integrated optimized control of the AC-DC converters for overload relief was shown to be fast in the system-wide mitigation of line congestion as triggered by contingencies in AC-DC grids. On a personal computer, the whole process implemented as a code of Matlab R2020b took just 20 seconds, while the nonlinear counterpart needed 92 minutes. Thus, the proposed method also lends itself to online application in practice. At the same time, the accuracy of the AC-DC linear power flow calculation results is consistent with the one reported for linear contingency analysis of just AC power transmission grids. As such, the proposed methodology of contingency analysis and control was proven to be efficient and valuable in contributing to power system security analysis of modern grids integrating AC and multi-terminal DC power transmission.

APPENDIX

A. Calculation of PTDF for DC Grids

From (9b), the change of flow over DC line l to a change of power injection at bus s and opposite change at bus r is determined by:

$$\frac{\partial P_{\mathrm{DC},l}}{\partial P^{\mathrm{inj}}_{\mathrm{DC},s}} - \frac{\partial P_{\mathrm{DC},l}}{\partial P^{\mathrm{inj}}_{\mathrm{DC},r}} = \frac{1}{r_{\mathrm{DC},ij}}\Big(\big(\frac{\partial v_{\mathrm{DC},i}}{\partial P^{\mathrm{inj}}_{\mathrm{DC},s}} - \frac{\partial v_{\mathrm{DC},j}}{\partial P^{\mathrm{inj}}_{\mathrm{DC},s}}\big) - \big(\frac{\partial v_{\mathrm{DC},i}}{\partial P^{\mathrm{inj}}_{\mathrm{DC},r}} - \frac{\partial v_{\mathrm{DC},j}}{\partial P^{\mathrm{inj}}_{\mathrm{DC},r}}\big)\Big). \quad (54)$$

The DC voltage differences $v_{\mathrm{DC},i}$ and $v_{\mathrm{DC},j}$ are obtained from (8b):

$$v_{\mathrm{DC},i} = R_{\mathrm{DC},i1}P^{\mathrm{inj}}_{\mathrm{DC},1} + \ldots + R_{\mathrm{DC},is}P^{\mathrm{inj}}_{\mathrm{DC},s} + \ldots + R_{\mathrm{DC},ir}P^{\mathrm{inj}}_{\mathrm{DC},r} + \ldots + R_{\mathrm{DC},i(n_{\mathrm{DC}}-1)}P^{\mathrm{inj}}_{\mathrm{DC},(n_{\mathrm{DC}}-1)} \quad (55)$$

$$v_{\mathrm{DC},j} = R_{\mathrm{DC},j1}P^{\mathrm{inj}}_{\mathrm{DC},1} + \ldots + R_{\mathrm{DC},js}P^{\mathrm{inj}}_{\mathrm{DC},s} + \ldots + R_{\mathrm{DC},jr}P^{\mathrm{inj}}_{\mathrm{DC},r} + \ldots + R_{\mathrm{DC},j(n_{\mathrm{DC}}-1)}P^{\mathrm{inj}}_{\mathrm{DC},(n_{\mathrm{DC}}-1)}. \quad (56)$$

Thus, the derivatives of the DC bus voltages with respect to bus power injections are given by:

$$\frac{\partial v_{\mathrm{DC},i}}{\partial P^{\mathrm{inj}}_{\mathrm{DC},s}} = R_{\mathrm{DC},is} \quad (57) \qquad \frac{\partial v_{\mathrm{DC},j}}{\partial P^{\mathrm{inj}}_{\mathrm{DC},s}} = R_{\mathrm{DC},js} \quad (58)$$

$$\frac{\partial v_{\mathrm{DC},i}}{\partial P^{\mathrm{inj}}_{\mathrm{DC},r}} = R_{\mathrm{DC},ir} \quad (59) \qquad \frac{\partial v_{\mathrm{DC},j}}{\partial P^{\mathrm{inj}}_{\mathrm{DC},r}} = R_{\mathrm{DC},jr}. \quad (60)$$

Inserting (57) to (60) into (54), the PTDF for DC grids in (61) is obtained:

$$PTDF_{\mathrm{DC},lsr} = \frac{1}{r_{\mathrm{DC},ij}}\big((R_{\mathrm{DC},is} - R_{\mathrm{DC},js}) - (R_{\mathrm{DC},ir} - R_{\mathrm{DC},jr})\big) \quad (61)$$

For the case where r is the reference bus, the entries $R_{\mathrm{DC},ir}$ and $R_{\mathrm{DC},jr}$ are omitted, leading to (19).

B. Calculation of LODF for AC and DC Grids

The LODF for AC grids is a function of PTDFs. The LODF measuring the change of flow over line l due to the outage of line m is given by [13]:

$$LODF_{\mathrm{AC},lm} = \frac{PTDF_{\mathrm{AC},lsr}}{1 - PTDF_{\mathrm{AC},msr}} \quad (62)$$

where buses s and r were originally connected by line m. In the special case where the outage of line m leads to islanding, then $PTDF_{\mathrm{AC},msr} = 1$, and (62) is not defined. To handle this issue, the LODF may be set to zero [13].

The derivation of a formula for the case of the DC grid is inspired from the procedure that led to (62). Fig. 5(a) shows DC line m, which is connected to the remainder of the grid through fictitious breakers at bus s and bus r, respectively. The outage of line m can be modeled by the opening of the fictitious breakers as depicted in Fig. 5(b). Alternatively, the outage may be modeled without changing the network topology as illustrated in Fig. 5(c). For this purpose, power $\widetilde{P}_{\mathrm{DC},m}$ is injected into bus s and $-\widetilde{P}_{\mathrm{DC},m}$ is injected into bus r so that $\widetilde{P}_{\mathrm{DC},m}$ flows over DC line m. Thanks to those injections, there are no power flows over the breakers even if they remain closed – effectively representing the outage of line m as far as the remainder of the grid is concerned. The modified flow $\widetilde{P}_{\mathrm{DC},m}$ is specified by applying the PTDF:

$$\widetilde{P}_{\mathrm{DC},m} = P^{0}_{\mathrm{DC},m} + PTDF_{\mathrm{DC},msr}\widetilde{P}_{\mathrm{DC},m}. \quad (63)$$

Assuming that $PTDF_{\mathrm{DC},msr} \neq 1$, (63) is rewritten as:

$$\widetilde{P}_{\mathrm{DC},m} = \frac{1}{1 - PTDF_{\mathrm{DC},msr}}P^{0}_{\mathrm{DC},m}. \quad (64)$$

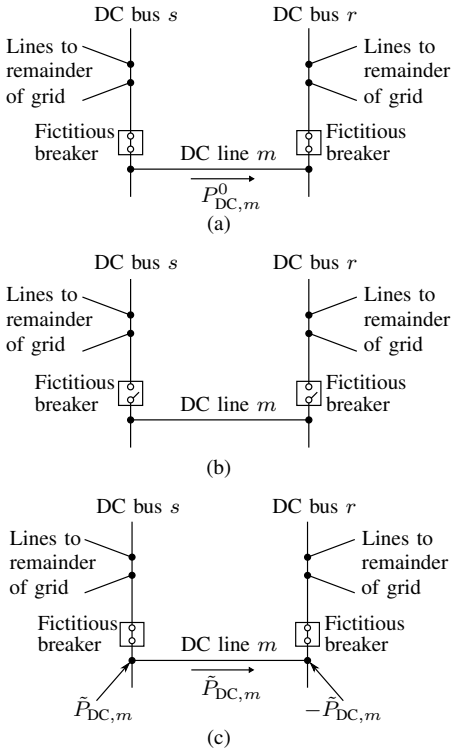

Fig. 5. Model of DC line outage; (a) before outage of line m; (b) outage of line m; (c) model of outage of line m for contingency analysis with no power flow through fictitious breakers. Modified from [13].

The outcome of (64) is used to calculate the power flow over any line l in the remainder of the grid:

$$\widetilde{P}_{\mathrm{DC},l} = P^0_{\mathrm{DC},l} + PTDF_{\mathrm{DC},lsr}\widetilde{P}_{\mathrm{DC},m}. \tag{65}$$

Inserting (64) into (65), the power flow over line l can be expressed as follows:

$$\widetilde{P}_{\mathrm{DC},l} = P^0_{\mathrm{DC},l} + LODF_{\mathrm{DC},lm}P^0_{\mathrm{DC},m} \tag{66}$$

with the newly formulated LODF for DC grids given by:

$$LODF_{\mathrm{DC},lm} = \frac{PTDF_{\mathrm{DC},lsr}}{1 - PTDF_{\mathrm{DC},msr}}. \tag{67}$$

For special cases, the same applies as stated for (62). The final expression of the LODF for DC grids is obtained by inserting (61) into (67):

$$LODF_{\mathrm{DC},lm}=\frac{\frac{1}{r_{\mathrm{DC},ij}}\big((R_{\mathrm{DC},is}-R_{\mathrm{DC},js})-(R_{\mathrm{DC},ir}-R_{\mathrm{DC},jr})\big)}{1-\frac{1}{r_{\mathrm{DC},sr}}\big((R_{\mathrm{DC},ss}-R_{\mathrm{DC},rs})-(R_{\mathrm{DC},sr}-R_{\mathrm{DC},rr})\big)}. \tag{68}$$

C. Parameters of modified IEEE 39-bus System

The parameters of the IEEE AC-DC 39+6-bus system are modified from [30], [31]. The base apparent power is set to 1000 MVA, the base voltage for the AC grid part is 345 kV, and the base voltage for the DC grid part is 645 kV. The series reactances, the series resistances, the shunt susceptances, and the limits for real power flows of AC transmission lines are given in Table VI. The series reactances, the series resistances, the tap ratios, and the limits for real power flows of transformers are summarized in Table VII. The series resistances and the flow limits of DC transmission lines are given in Table VIII. The real and reactive power injections at AC buses, and the set voltage magnitudes for the considered grid operating points are presented in Table IX.

TABLE VI
PARAMETERS OF AC TRANSMISSION LINES IN AC-DC 39+6-BUS SYSTEM

Bus connection	Series reactance [p.u.]	Series resistance [p.u.]	Shunt susceptance [p.u.]	Real power flow limit [MW]
A1-A2	0.411	0.035	0.0699	600
A1-A39	0.250	0.010	0.0750	1000
A2-A3	0.151	0.013	0.0257	500
A2-A25	0.086	0.070	0.0146	500
A3-A4	0.213	0.013	0.0221	500
A3-A18	0.133	0.011	0.0214	500
A4-A14	0.129	0.008	0.0138	500
A8-A9	0.363	0.023	0.0380	900
A9-A39	0.250	0.010	0.1200	900
A10-A11	0.043	0.004	0.0073	600
A10-A13	0.043	0.004	0.0073	600
A13-A14	0.101	0.009	0.0172	600
A14-A15	0.217	0.018	0.0366	600
A15-A16	0.094	0.009	0.0171	600
A16-A17	0.089	0.007	0.0134	600
A16-A19	0.195	0.016	0.0304	600
A16-A21	0.135	0.008	0.0255	600
A16-A24	0.059	0.003	0.0068	600
A17-A18	0.082	0.007	0.0132	600
A17-A27	0.173	0.013	0.0322	600
A21-A22	0.140	0.008	0.0257	900
A22-A23	0.096	0.006	0.0185	600
A23-A24	0.350	0.022	0.0361	600
A25-A26	0.323	0.032	0.0531	600
A26-A27	0.147	0.014	0.0240	600
A26-A28	0.474	0.043	0.0780	600
A26-A29	0.625	0.057	0.1029	600
A28-A29	0.151	0.014	0.0249	600
A11-A13	0.001	0.000	0.0000	1000

TABLE VII
PARAMETERS OF TRANSFORMERS IN AC-DC 39+6-BUS SYSTEM

Bus connection	Series reactance [p.u.]	Series resistance [p.u.]	Tap ratio [p.u.]	Real power flow limit [MW]
A2-A30	0.181	0.000	1.025	900
A10-A32	0.200	0.000	1.070	1200
A12-A11	0.435	0.016	1.006	500
A12-A13	0.435	0.016	1.006	500
A19-A20	0.138	0.007	1.060	900
A19-A33	0.142	0.007	1.070	900
A20-A34	0.180	0.009	1.009	900
A22-A35	0.143	0.000	1.025	900
A23-A36	0.272	0.005	1.000	900
A25-A37	0.232	0.006	1.025	900
A29-A38	0.156	0.008	1.025	1200

The applied converter station models are governed by (10) to (13) in Section II-B. The real power injections from the converters into the AC and DC grid buses occur according to (10). The initial operating point was selected such that the real power injections of converters C1 to C4 are controlled to specified values, given by the first four entries of (52). The real power injection of C5 into the AC grid ensures power balance in the DC grid part with the DC bus voltage of C5 controlled to a set value. Thus, for this type of control, D5 acts as a slack bus in the DC grid part with a bus voltage at 1 p.u.. For the linear power flow calculus, the power balance in the DC grid part is maintained via (14). For consistency with the applied converter controls, AC buses A7 and A31 are to serve as slack buses. Beyond that, A39 serves as a slack bus. As such, the power injections for those buses listed in Table IX are modified.

Since the converters considered are realized through modular

TABLE VIII
PARAMETERS OF DC TRANSMISSION LINES IN AC-DC 39+6-BUS SYSTEM

Bus connection	Resistance [p.u.]	Real power flow limit [MW]
D2-D3	0.065	480
D2-D6	0.036	600
D3-D4	0.025	480
D1-D6	0.033	900
D1-D5	0.015	900
D4-D6	0.009	1200
D4-D5	0.027	900

TABLE IX
PARAMETERS OF AC BUSES IN AC-DC 39+6-BUS SYSTEM

Bus	Real power injection [MW]	Reactive power injection [MVAr]	Voltage [p.u.]
A1	−97.6	−44.2	
A3	−322.0	−2.4	
A4	−1000.0	−184.0	
A7	−233.8	−84.0	
A8	−1000.0	−176.6	
A9	−6.5	−66.6	
A12	−8.5	−88.0	
A15	−320.0	−153.0	
A16	−329.0	−32.3	
A18	−158.0	−30.0	
A20	−680.0	−103.0	
A21	−274.0	−115.0	
A23	−247.5	−84.6	
A24	−308.6	92.2	
A25	−224.0	−47.2	
A26	−139.0	−17.0	
A27	−281.0	−75.5	
A28	−206.0	−27.6	
A29	−283.5	−26.9	
A30	250.0		1.050
A31	990.8		0.982
A32	1170.0		0.984
A33	642.0		0.997
A34	518.0		1.012
A35	660.0		1.049
A36	570.0		1.064
A37	550.0		1.028
A38	840.0		1.027
A39	−104.0		1.030

multilevel converter technology, filters are not needed since sinusoidal waveforms are closely approximated. Voltages inside the converters can be calculated by considering relevant transformer and arm reactances, which are chosen at 0.16 p.u. and 0.13 p.u., respectively, for a base apparent power of 1000 MVA and a base voltage of 345 kV. Reactive power injections into the AC grid part are set to zero, and those settings are only relevant for the nonlinear power flow calculus.

REFERENCES

[1] Global Wind Energy Council, "Global wind report 2022," Brussels, Belgium, Tech. Rep., 2022.

[2] K. Strunz, M. Kuschke, and S. Schilling, "Climate-friendly and socially inclusive AC-DC renewable energy system with overlay multi-terminal HVDC network (OVANET): Solution with fully distributed optimization and infrastructure combination," *Int. J. Electr. Power Energy Syst.*, vol. 132, pp. 106–119, Nov. 2021.

[3] C.-K. Kim *et al.*, *HVDC Transmission: Power Conversion Applications in Power Systems*. Singapore: Wiley, 2009.

[4] S. Schilling, M. Kuschke, and K. Strunz, "AC-DC optimal power flow implementation: Modeling and application to an HVDC overlay grid," in *IEEE PowerTech*, Manchester, Great Britain, Jun. 2017, pp. 1–6.

[5] L. Zhang *et al.*, "Modeling, control, and protection of modular multilevel converter-based multi-terminal HVDC systems: A review," *CSEE J. Power Energy Syst.*, vol. 3, no. 4, pp. 340–352, Dec. 2017.

[6] H. Xie, Z. Bie, and G. Li, "Reliability-oriented networking planning for meshed VSC-HVDC grids," *IEEE Trans. Power Syst.*, vol. 34, no. 2, pp. 1342–1351, Mar. 2019.

[7] J. A. Ansari, C. Liu, and S. A. Khan, "MMC based MTDC grids: A detailed review on issues and challenges for operation, control and protection schemes," *IEEE Access*, vol. 8, pp. 168 154–168 165, 2020.

[8] R. Martínez-Parrales, C. R. Fuerte-Esquivel, B. A. Alcaide-Moreno, and E. Acha, "A VSC-based model for power flow assessment of multi-terminal VSC-HVDC transmission systems," *J. Mod. Power Syst. Clean Energy*, vol. 9, no. 6, pp. 1363–1374, Nov. 2021.

[9] Q. Li and N. Zhao, "General power flow calculation for multi-terminal HVDC system based on sensitivity analysis and extended AC grid," *IEEE Trans. Sustain. Energy*, vol. 13, no. 4, pp. 1886–1899, Oct. 2022.

[10] Y. Chen, R. Moreno, G. Strbac, and D. Alvarado, "Coordination strategies for securing AC/DC flexible transmission networks with renewables," *IEEE Trans. Power Syst.*, vol. 33, no. 6, pp. 6309–6320, Nov. 2018.

[11] Z. Zhu, J. Yan, C. Lu, Z. Chen, and J. Tian, "Two-stage coordinated control strategy of AC/DC hybrid power system based on steady-state security region," *IEEE Access*, vol. 8, pp. 139 221–139 243, 2020.

[12] B. O. Adewolu and A. K. Saha, "Contingency control capability of an optimized HVDC-based VSC transmission system," *IEEE Access*, vol. 9, pp. 4112–4128, 2021.

[13] A. J. Wood, B. F. Wollenberg, and G. B. Sheblé, *Power Generation, Operation and Control*. Hoboken, NJ, USA: Wiley, 2014.

[14] A. Gupta, G. Gurrala, and P. S. Sastry, "An online power system stability monitoring system using convolutional neural networks," *IEEE Trans. Power Syst.*, vol. 34, no. 2, pp. 864–872, Mar. 2019.

[15] R. Yan, G. Geng, and Q. Jiang, "Data-driven transient stability boundary generation for online security monitoring," *IEEE Trans. Power Syst.*, vol. 36, no. 4, pp. 3042–3052, Jul. 2021.

[16] J. Cao, W. Du, and H. F. Wang, "An improved corrective security constrained OPF for meshed AC/DC grids with multi-terminal VSC-HVDC," *IEEE Trans. Power Syst.*, vol. 31, no. 1, pp. 485–495, Jan. 2016.

[17] K. Meng *et al.*, "Hierarchical SCOPF considering wind energy integration through multi-terminal VSC-HVDC grids," *IEEE Trans. Power Syst.*, vol. 32, no. 6, pp. 4211–4221, Nov. 2017.

[18] Y. Li and Y. Li, "Security-constrained multi-objective optimal power flow for a hybrid AC/VSC-MTDC system with lasso-based contingency filtering," *IEEE Access*, vol. 8, pp. 6801–6811, 2019.

[19] J. S. Guzmán-Feria, L. M. Castro, N. Guzmán-Cabrera, and J. Tovar-Hernández, "Security constrained OPF for AC/DC systems with power rescheduling by power plants and VSC stations," *Sustainable Energy, Grids and Networks*, vol. 27, Sep. 2021.

[20] B. Stott, J. Jardim, and O. Alsac, "DC power flow revisited," *IEEE Trans. Power Syst.*, vol. 24, no. 3, pp. 1290–1300, Aug. 2009.

[21] J.-C. Fernández-Pérez, F. M. Echavarren Cerezo, and L. Rouco Rodríguez, "Linear power flow algorithm with losses for multi-terminal VSC AC/DC power systems," *IEEE Trans. Power Syst.*, vol. 37, no. 3, pp. 1739–1749, May 2022.

[22] L. M. Castro, E. Acha, and J. R. Rodriguez-Rodriguez, "Efficient method for the real-time contingency analysis of meshed HVDC power grids fed by VSC stations," *IET Gener. Transm. Distrib.*, vol. 12, no. 13, pp. 3158–3166, Jul. 2018.

[23] E. Iggland, R. Wiget, S. Chatzivasileiadis, and G. Anderson, "Multi-area DC-OPF for HVAC and HVDC grids," *IEEE Trans. Power Syst.*, vol. 30, no. 5, pp. 2450–2459, Sep. 2015.

[24] Z. Yuan, Y. Wang, Y. Yi, C. Wang, Y. Zhao, and W. Wen, "Fast linear power flow algorithm for the study of steady-state performance of DC grid," *IEEE Trans. Power Syst.*, vol. 34, no. 6, pp. 4240–4248, Nov. 2019.

[25] Y. C. Chen, A. D. Domínguez-García, and P. W. Sauer, "Measurement-based estimation of linear sensitivity distribution factors and applications," *IEEE Trans. Power Syst.*, vol. 29, no. 3, pp. 1372–1382, May 2014.

[26] M. Liu and G. Gross, "Role of distribution factors in congestion revenue rights applications," *IEEE Trans. Power Syst.*, vol. 19, no. 2, pp. 802–810, May 2004.

[27] P. Wang, M. Kuschke, and K. Strunz, "Equal-area criterion and analytical model for transient stability assessment of hybrid AC–DC transmission system using voltage sourced converter," *IET Renew. Power Gener.*, vol. 17, pp. 18–35, 2023.

[28] ——, "Analytical modeling of modular multilevel converter under pole-to-pole DC fault and application to system design and protection," *IEEE Trans. Energy Convers.*, vol. 37, no. 4, pp. 2722–2736, Dec. 2022.

[29] S. J. Wright, *Primal-Dual Interior-Point Methods*. Philadelphia, PA, USA: Society for Industrial and Applied Mathematics, 1997.

[30] F. B. Ajaei and R. Iravani, "Dynamic interactions of the MMC-HVDC grid and its host AC system due to AC-side disturbances," *IEEE Trans. Power Del.*, vol. 31, no. 3, pp. 1289–1298, Jun. 2016.

[31] M. A. Pai, *Energy Function Analysis for Power System Stability*. Norwell, MA, USA: Springer US, 1989.

[32] J. Beerten and R. Belmans, "Development of an open source power flow software for high voltage direct current grids and hybrid AC/DC systems: MATACDC," *IET Gener. Transm. Distrib.*, vol. 9, no. 10, pp. 966–974, Jul. 2015.

[33] "Network Code for Requirements for Grid Connection Applicable to all Generators," ENTSO-E, Brussels, Belgium, Tech. Rep., 2013.
[34] D. J. Mundform *et al.*, "Number of replications required in Monte Carlo simulation studies: A synthesis of four studies," *J. Mod. Appl. Stat. Methods*, vol. 10, no. 1, pp. 19–28, May 2011.

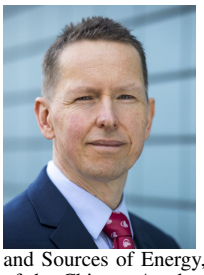

Kai Strunz received the Dipl.-Ing. and Dr.-Ing. (summa cum laude) degrees from Saarland University, Saarbrücken, Germany, in 1996 and 2001, respectively. From 1995 to 1997, he pursued research at Brunel University in London. From 1997 to 2002, he worked at the Division Recherche et Développement of Electricité de France in the Paris area. From 2002 to 2007, he was an Assistant Professor of electrical engineering with the University of Washington in Seattle. Since September 2007, he has been Professor with the Department of Sustainable Electric Networks and Sources of Energy, Technische Universität Berlin. He is Guest Professor of the Chinese Academy of Science, Beijing.

Dr. Strunz is the Chair of the IEEE Power and Energy Society (PES) Committee on Energy Development and Power Generation, Chair of the Subcommittee on Distributed Energy Resources, and Chair of the Working Group on Dynamic Performance and Modeling of HVDC Systems and Power Electronics for Transmission Systems. In 2012, Dr. Strunz was the General and Technical Program Chair of the IEEE PES Innovative Smart Grid Technologies (ISGT) Europe 2012 in Berlin. He received the IEEE PES Prize Paper Awards in 2015 and 2023, and the Journal of Emerging and Selected Topics in Power Electronics First Prize Paper Award in 2015.

Samuel Schilling received the B. Sc. and the M. Sc. degrees in electrical engineering from Technische Universität (TU) Berlin, Germany, in 2014 and 2015, respectively. His research interests include security and operation of integrated AC-DC power grids. In 2022, he joined 50Hertz Transmission, Berlin. In 2016, Samuel Schilling received the VDI award for his outstanding study performance from the Association of German Engineers.

Maren Kuschke received the Dipl.-Ing. and Dr.-Ing. (summa cum laude) degrees from Technische Universität (TU) Berlin, Germany, in 2008 and 2014, respectively. She studied electrical engineering with focus on electrical drives, photovoltaics, and electric energy systems at TU Berlin and KTH Stockholm, Sweden. Maren Kuschke received the VDI Award from the Association of German Engineers in 2009 and the IEEE PES German Chapter Best Master Thesis Award in 2010. She is recipient of the IEEE PES Prize Paper Award 2015.

Anna Czerwinska received the B. Sc. and the M. Sc. degrees in electrical engineering from Technische Universität (TU) Berlin, Germany, in 2018 and 2020, respectively. She is currently pursuing her Ph.D. degree at TU Berlin, focusing on optimization of large-scale power systems with a high share of renewable energy. For her master thesis, she received the Clara-von-Simson Prize and the TU Berlin Faculty Prize in 2021.